

Electrochemical Local Maskless Micro/Nanoscale Deposition, Dissolution, and Oxidation of Metals and Semiconductors (A Review)

A. D. Davydov^{a, *} and V. M. Volgin^{a, b, **}

^a*Frumkin Institute of Physical Chemistry and Electrochemistry, Russian Academy of Sciences, Moscow, 119071 Russia*

^b*Tula State University, Tula, 300012 Russia*

**e-mail: davydov@elchem.ac.ru*

***e-mail: volgin@tsu.tula.ru*

Received March 26, 2019; revised May 3, 2019; accepted July 6, 2019

Abstract—The review is devoted to the modern methods of local maskless electrochemical machining of metals and semiconductors with the aim of formation of individual islands or cavities, their groups, and patterns according to a given program on their surface, or 3D micro/nanostructures, for example, metal threads and various thread structures. For this purpose, various methods of localizing the electrochemical deposition, dissolution, or oxidation are used.

Keywords: local electrodeposition, local etching, oxidation, micro/nanostructures, scanning probe microscope, laser-assisted electrochemical machining

DOI: 10.1134/S1023193520010036

CONTENT

1. Introduction
 2. Electrochemical deposition, dissolution, and oxidation with micro/nano tool-electrodes (TE) and interelectrode distances
 - 2.1. Electrochemical dissolution of metal with thin-rod tool-electrode
 - 2.2. Application of ultrashort pulses to enhance the localization of process
 - 2.3. The formation of metal threads and more complex microstructures with a moving microdisk tool-electrode
 - 2.4. Application of scanning probe microscopes (SPM)
 3. Electrochemical deposition and dissolution using tool-electrode in micro/nanopipettes and nozzles
 - 3.1. Formation of microstructures with moving microelectrode in free pipette through liquid meniscus
 - 3.2. Formation of metal microstructures with moving microelectrode in pipette immersed into electrolyte
 - 3.3. Metal electrodeposition using SPM with a probe in the form of micropipette with electrolyte
 - 3.4. Application of electrochemical microcells for local ECM of metals
 - 3.5. Jet electrochemical micromachining.
 4. Localization of electroactive component of electrolyte in the machining zone
 - 4.1. Local metal electrodeposition with soluble anode
 - 4.2. Local metal electrodeposition with insoluble anode. Method of chemical lenses
 - 4.3. Local etching of metals and semiconductors in the positive feedback mode
 - 4.4. Local etching of metals and semiconductors. Confined etchant layer technique
 - 4.5. Local electrodeposition of metal with non-electrode SPM probe
 5. Laser-assisted electrochemical (LAECM) and laser-jet electrochemical machining
 - 5.1. Effect on equilibrium potential
 - 5.2. Increase of reaction rate controlled by charge transfer
 - 5.3. Intensification of mass transfer in the diffusion boundary layer
 - 5.4. Effect on current efficiency
 - 5.5. Effect on metal passivity
 - 5.6. Thermal stresses and plastic deformation in the surface metal layer
 - 5.7. LAECM of semiconductors
 - 5.8. Laser-jet electrochemical machining
 6. Conclusions
- ## 1. INTRODUCTION
- Various schemes of electrochemical machining are used to form the nano- and micro-structured surface

and 3D microstructures [1–3]. They have several important advantages: the absence of mechanical and heat impacts on the workpiece (except for the laser-assisted electrochemical machining), no tool wear, wide possibilities for controlling the shape and dimensions of microstructures by varying the machining modes, relative simplicity and low cost of electrochemical machining (ECM) processes, and good reproducibility of results.

The methods of micro/nano-ECM are divided into subtractive and additive. In the first case, the structured surface is formed as a result of local removal of material from the original workpiece; in the second case, it is formed as a result of local electrodeposition of material onto the surface of original workpiece [4].

The methods of micro/nano-ECM found application for manufacturing microelectromechanical systems, where miniature mechanical components are combined with electronic circuits, and other modern technologies.

The method of local electrochemical oxidation of metals and semiconductors is important for solving microelectronic problems.

Maskless technologies enable avoiding the multi-stage engineering processes of ECM, where the localization is provided by partial protecting workpiece surface with masks, primarily, photoresistive masks.

Typical problems of micro/nano-ECM are the formation of microwires, metal threads, columns with a high aspect ratio (the ratio of wire length to its diameter), the formation of individual islands or cavities and their groups on the metal substrates, patterning with lines of the desired shape and dimensions using the electrodeposition, dissolution or oxidation of metals by moving the tool-electrode (TE) over the substrate surface along a prescribed trajectory. As a result, 1D, 2D, and 3D structures can be obtained. The same methods are used for microstructuring of semiconductor surface.

The localization of electric field by using micro-electrode TE and micron and submicron interelectrode distances is the main method for localization of electrochemical metal deposition, dissolution, and oxidation in the micro- and nanoscales. The micro-electrode can be in the form of a needle, a wire end-face, a capillary filled with an electrolyte with a counter-electrode inside it, or a specially adapted probe of scanning probe microscope (SPM). A number of additional localization techniques are developed and used. These are special electric modes (ultrashort pulses), the localization of active component of the electrolyte in the working zone, for example, in the electrolyte “tube” between the microelectrode and workpiece surface microarea, and laser radiation focused at the specified “point” on the workpiece surface.

The practical application of the methods of micro- and nano-electrochemical machining of metals requires special equipment. Commonly, the work-

piece (WP) is fixed on a horizontal two-coordinate table that allows one to place WP in the required position relative to the vertically located TE or move WP according to a given program to create the desired pattern on it. There are a device for high-precision (up to several nm) positioning of TE at a given distance from WP, a power source, and a system for controlling all process parameters.

The local electrodeposition is carried out in the electrochemical cells of various types under the potentiostatic or galvanostatic conditions, in the pulsed modes according to two-, three-, or four-electrode scheme using adjustable power sources, potentiostats, and bipotentiostats. The use of bipotentiostats enables maintaining independent potentials of probe and substrate against a common reference electrode. A scheme without connecting the substrate to an external power source is also used; here, the workpiece potential is applied using a certain redox pair in the solution.

The local deposition for fabricating micro/nano-structures is performed in the same electrolytes that are commonly used in the traditional electroplating. Solutions of acids, alkalis, or salts are used for the local dissolution.

Some methods of local ECM presented in the review have already found practical application, whereas other methods show their various potentialities and are of great scientific interest.

2. ELECTROCHEMICAL DEPOSITION, DISSOLUTION, AND OXIDATION WITH MICRO/NANO TOOL-ELECTRODES AND INTERELECTRODE DISTANCES

2.1. *Electrochemical Dissolution of Metal with Thin-Rod Tool-Electrode*

Tool-electrodes (TE) in the form of a thin rod, frequently made of tungsten or WC, are widely used for the anodic dissolution. In the course of electrochemical micromachining, TE moves along a given trajectory (Fig. 1). In different cases, its side surface can be free from insulation or protected by an insulating layer except for a tip of a certain length.

This method enables one to apply various patterns onto the metal surfaces, perform microstructuring of the surface and electrochemical engraving operations.

In the works on the direct local electrochemical dissolution of metals, not only thin cylindrical or needle-shaped tool-electrodes are used. The application of TE with a microspherical or microdisk tip raises the degree of localization and stability of machining [5–7].

Ultrashort pulses of duration from several units to several hundred nanoseconds are commonly used in works in this field [7–12]. This is explained in the next section of the review. Aqueous solutions of acids (HCl, H₂SO₄) [7, 8, 10] and nonaqueous, for example, alco-

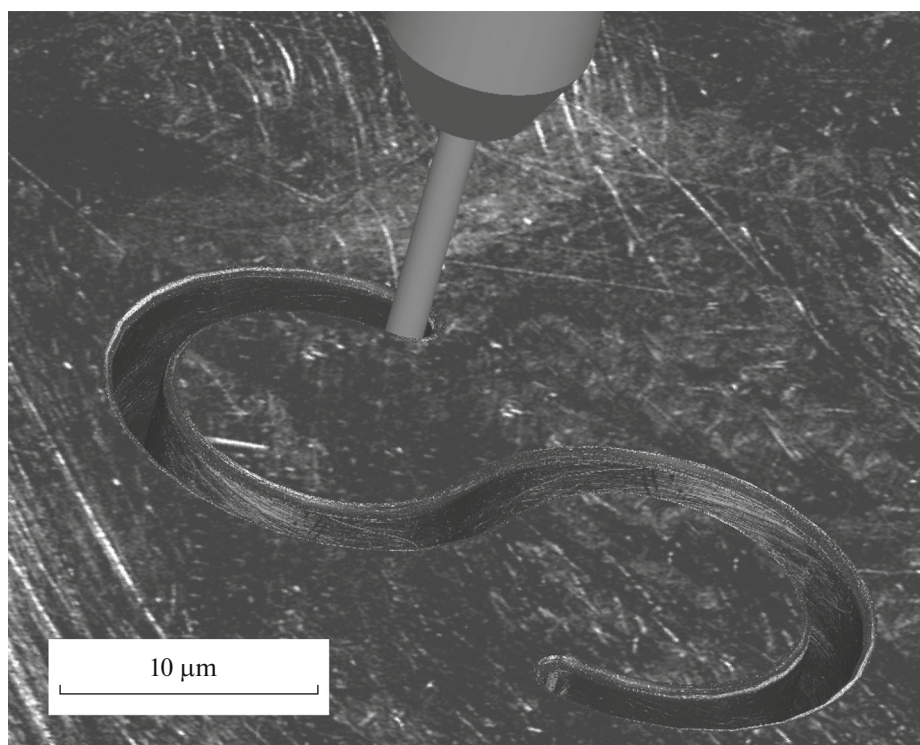


Fig. 1. Example of local electrochemical metal dissolution with tool-electrode in the shape of thin rod.

hol solutions (HClO_4 , NaBr) [9, 12] are commonly used for ECM of various materials by this method.

Lee et al. [13] described an electrode device for micro-ECM containing more than hundred elements, columns 800 μm in length of square, triangular or circular cross-section 100 μm in diameter to obtain simultaneously the same number of holes in the nickel plate. The centers of neighboring elements are 300 μm distant. The side surface of each element is coated with an insulating composition in order to enhance the accuracy of machining. During the machining, the interelectrode distance (gap) is 10–20 μm and, in some cases, even smaller. In this case, the removal of the products of electrode reactions during the machining is significantly hampered as compared to machining with a single rod TE. To solve this problem, it is proposed to use a special mode, which was developed for a conventional ECM many years ago and was called pulse–cyclic ECM [14–16]. In this method, cyclic variation of TE position relative to the workpiece is synchronized with a series of short voltage pulses. Several versions of synchronization are developed. For example, TE is brought to touch with WP; then, removed to a prescribed distance (working interelectrode distance) and a series of short pulses is imposed (machining); then, TE is removed to a larger distance to wash the interelectrode space with the electrolyte flow in the absence of current; TE is again brought to touch with WP and so on. In [13], a series of short voltage pulses was imposed at the working

interelectrode distance, and the pauses in the current were corresponded to the periods when TE was removed from WP and returned to the working interelectrode distance. The authors of [13] demonstrated a high efficiency of this method by the example of ECM of a series of microholes of various cross-section shapes with low taper (about 1.4°) in a nickel plate 100 μm thick. The pulse-on and pulse-off times were 20 μs . The process was performed in 0.25 M NaClO_3 solution.

A similar problem of facilitating the removal of electrode reaction products during the pulsed ECM with very small gaps by an electrode device with several tens of microwire elements was solved in [17] using a vibrating electrode device. Vibration is synchronized with the imposed voltage pulses so that the pulses are applied in those short time intervals when TE is at small distances from WP, the pauses between the pulses coincide with the time periods when TE is removed from WP to wash the interelectrode space. This work gives the examples of ECM for fabricating holes and microscale gear wheels. The processes are performed in the 5% NaNO_3 solution at a pulse voltage of several volts and a frequency of 5 kHz. It is shown that an increase of the voltage to 5 V leads to an increase in the diameter and depth of the resulting holes. In contrast to the mode, which is widely used in the conventional (not micro/nano-) ECM with a vibrating electrode [14–16, 18], the authors of [17] do not use the forced electrolyte flow and add an abrasive powder to the NaNO_3 solution, as well as in the

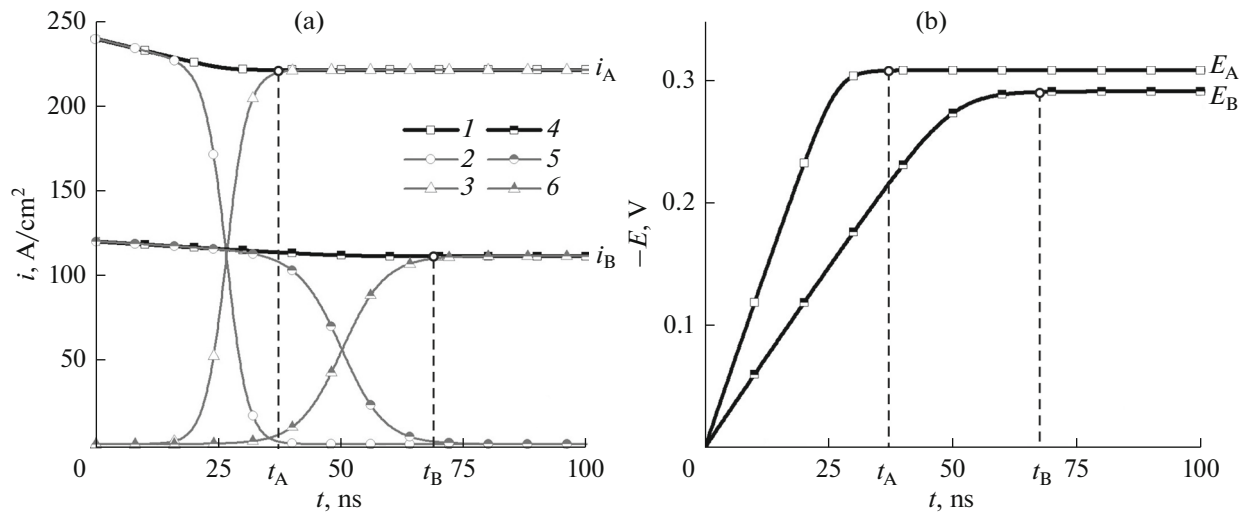


Fig. 2. (a) Schemes of time dependence of local currents (1–3) on the area with a smaller gap and (4–6) on the area with a larger gap during local copper electrodeposition in 1 M CuSO_4 after a given voltage was imposed and (b) the corresponding charging curves of electric double layer: (1 and 4) the total current density (squares); (2 and 5) the current density of charge—discharge of EDL capacitance (circles); and (3 and 6) Faradaic current density (triangles) at the voltage amplitude of 4 V and pulse duration of 100 ns.

conventional combined electrochemical and abrasive machining, for example [19]. This method is characterized by certain wear of TE in the course of machining.

The method of direct anodic dissolution with a sharpened W wire TE can be also applied to the micro-ECM of semiconductor materials with the proper choice of the electrolyte composition and machining mode [20, 21].

2.2. Application of Ultrashort Pulses to Enhance the Localization of Process

In many works on the micro/nano-ECM, the dissolution and deposition of metals are localized using the method based on the ultrashort (nanosecond) voltage pulses [22–24]. This method combined with a very small gap enables obtaining especially high degrees of localization.

Let us consider the mechanism of this method of process localization.

The voltage applied between TE and WP should provide overcoming ohmic resistance of the solution layer between the electrodes and the polarization of electrodes, which is required to reach sufficient rate of electrochemical reactions. The latter requires initial charging of electrical double layer (EDL) on the electrodes (we are interested in the electrode for its surface patterning). The ohmic potential drop is reached very quickly, whereas EDL is charged much slower. The characteristic time of charging bulk electrolyte solution (the time of reaching the ohmic potential drop) is

$$\lambda_D^2/D, \text{ where } \lambda_D = \sqrt{\frac{\varepsilon_0 \varepsilon_r RT}{F^2 \sum z_i^2 c_{i,b}}}$$

D is the diffusion coefficient of electroactive ion; ε_0 is

the electric constant; ε_r is the relative dielectric permeability of solution; R is the gas constant; T is the temperature of solution; F is the Faraday constant; z_i , and $c_{i,b}$ are the charge and bulk concentration of ions of the i -th type, respectively. For example, for 1 : 1 electrolyte with concentration of 1 M ($\lambda_D \approx 3 \times 10^{-10}$ m) and the diffusion coefficients of 10^{-9} m^2/s , we obtain the characteristic time of ohmic potential drop in the

solution of $(3 \times 10^{-10})^2 / 10^{-9} \approx 10^{-10}$ s = 0.1 ns. At the same time, the characteristic EDL charging time is

$$\frac{2RTC}{nFi_F^\infty} \ln \frac{i_F^\infty}{i_0},$$

where C is the specific capacitance of EDL; i_0 is the exchange current density; and i_F^∞ is the steady-state Faradaic current density. At $C = 0.2$ F/ m^2 , $n = 2$, $i_0 = 1$ A/ cm^2 , and $i_F^\infty = 10$ A/ cm^2 , the characteristic EDL charging time is approximately 1000 ns.

With increasing i_0 and i_F^∞ , the characteristic EDL charging time decreases and, at $i_0 = 1$ A/ cm^2 and $i_F^\infty = 100$ A/ cm^2 , becomes approximately 20 ns. That is, in a very wide range of the system parameters, the time of ohmic potential drop is significantly shorter than the EDL charging time.

After imposing a voltage pulse, the current increases jumpwise (in the absence of diffusion limitations) to i_A (in the region with a smaller gap) and to i_B in the region with a larger gap (Fig. 2, curves 1 and 4).

However, the anodic potential varies relatively slowly (Fig. 2b) due to charging of EDL capacitance; only a fraction of currents i_A and i_B is consumed for this process (Fig. 2a, curves 2 and 5).

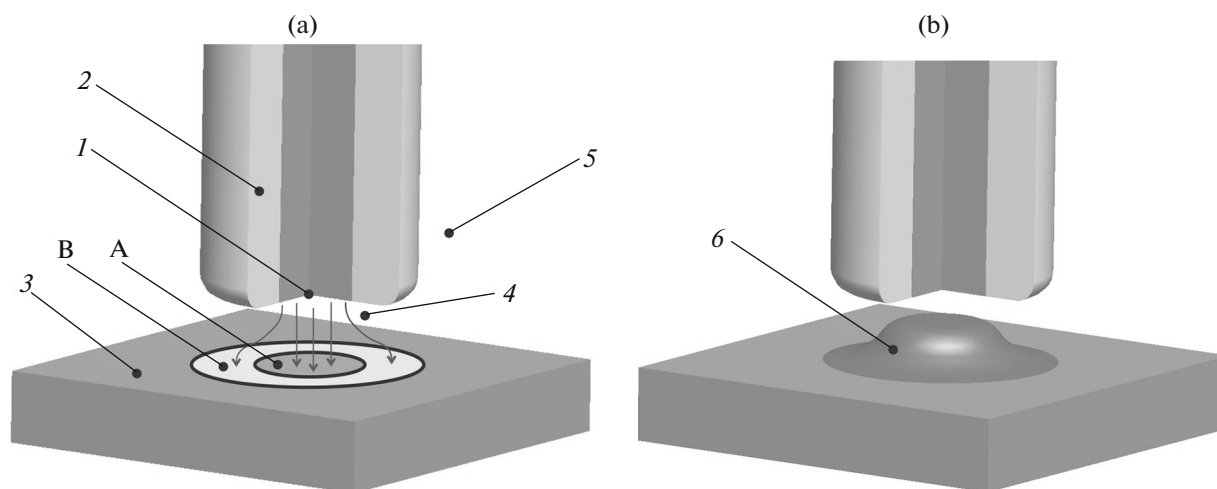


Fig. 3. Scheme of local electrodeposition using insoluble anode: (1) anode, (2) insulation of side anode surface, (3) substrate, (4) interelectrode gap, (5) electrolyte solution containing metal ions, and (6) micro/nano deposit of metal on substrate surface; (a) scheme of ECM with indicated working zone A and adjacent zone B on the substrate; (b) scheme with local electrodeposit (6).

Initially, the entire charge in a pulse is consumed for charging EDL (Fig. 2a, curves 2 and 5). As EDL is charged, the charge consumed for this process decreases and for the Faradaic process of metal deposition or dissolution increases (Fig. 2a, curves 3 and 6). At the time t_A , the charging in the region with a smaller gap is completed, the potential reaches a certain value E_A (Fig. 2b), which determines the current, which is entirely consumed for the Faradaic process at $t > t_A$ (Fig. 2b, $t > 35$ ns).

It is important that the EDL charging rate differs in the region on the substrate immediately below the TE (short straight current lines, Fig. 3, region A) and at a slightly larger distance (curved current lines, Fig. 3, region B). A potential drop in the solution is larger in region B than in region A. In region B, the steady-state electrode potential E_B is lower and is reached in a longer time t_B (Fig. 2b). Correspondingly, the current i_B is lower than i_A in the working zone, Fig. 2. In spite of small dimensions of local electrodeposition zone (the distance between the surface regions with the smallest and largest gaps is only several microns) and rather high conductivity of solution, the nonequipotentiality of workpiece surface reaches large values of several tens millivolts (Fig. 2b). This is due to very high current densities: they are by 3–5 orders of magnitude higher than the current densities in the traditional electrodeposition.

If the pulse-on time t_p is chosen to be equal to t_B , the difference between the dissolution (deposition) rates in region A and in some point in region B is determined by the polarization difference ($E_A - E_B$) in accordance, for example, with the well-known Tafel equation (a logarithmic increase of the current with increasing electrode potential).

A choice of $t_p < t_B$ leads to a larger difference between the local potentials, to a larger excess of the metal dissolution (deposition) rate in region A over the process rate in region B, i.e. to a higher degree of process localization.

At an optimal pulse-on time and sufficient pulse amplitude, in region A on the substrate, EDL will be completely charged and enough charge will remain for the metal dissolution. In region B, EDL will be only partially charged in the pulse-on time and a very small fraction of charge will be consumed for the metal deposition or dissolution.

Thus, by controlling the pulse duration (choosing t_p), a high degree of localization of the Faradaic process in region A on the substrate surface can be achieved.

It is clear that there is a critically short pulse-on time at a given amplitude, which will not provide sufficiently complete charging of EDL even in region A. Virtually the entire charge in the pulses will be consumed only for the periodic (with the frequency of pulse voltage) charging of EDL. The experimental results presented in [25] show the presence of a critical minimum pulse-on time. In this work, it is experimentally supported that the smaller is the working surface area of micro TE, the faster the highest machining rate is reached. It is concluded that the side surface of TE in the shape of a rod of small diameter should be insulated. The use of such an electrode reduces the taper of the hole formed by the local dissolution.

In [22–24], the method of ultrashort pulses was applied for the local metal dissolution or deposition using a low-frequency (a time constant of about 1 ms) bipotentiostat. The bipotentiostat independently maintains the given basic potentials of WP and TE against the reference electrode (platinum pseudo-reference electrode) using Pt counter electrode. The end

face of Pt or W wire serves as the tool-electrode. A series of voltage pulses, for example, with a pulse-on time of 50 ns and pulse-off time of 500 ns, is applied by the pulse generator onto WP. So short pulses have no effect on the operation of low-frequency bipotentiostat; therefore, using the pulse generator, the required polarization of WP can be realized in the region where the metal dissolution or deposition should be performed.

Such modes of ECM are characterized by relatively low productivity; however, they are advantageous in the processes of micro/nano-ECM, when a small amount of metal is removed and the productivity is not very important as compared to the accuracy, resolution of ECM.

The calculations and experiments showed [22, 23] that so short pulses can be chosen that at points located just a few microns away from the boundary of region A on the substrate (Fig. 3), virtually no dissolution or deposition occurs, whereas directly under TE, substantial dissolution or deposition takes place. The diameter of deposited metal island or dissolved region on the substrate is almost equal to the TE diameter. The authors of [22, 23] compare the time constant τ of EDL charging (the product of the electrolyte resistance by the EDL capacitance) with the voltage pulse duration t_p . An acceptable rate of dissolution or deposition for certain purpose is provided by the required pulse amplitude under the condition that τ does not substantially exceed t_p . The electrolyte resistance, and, consequently, τ are directly proportional to the interelectrode distance; therefore, it is possible to choose such t_p that a sufficient degree of EDL charging and the required Faradaic process rate will be achieved only at the smallest interelectrode gap (the lowest resistance).

In other words, the purpose of ultrashort pulses is that the main part of the pulse be occupied by the non-steady-state processes in the first short period of time after the power source is switched-on. At too long pulses, their main part is occupied by the steady state, when the difference in the dissolution rates in the end-face and side gaps is smaller.

Schuster et al. [22] used this method for localization of copper cathodic deposition from the 0.01 M HClO_4 + 0.1 M CuSO_4 solution on the gold substrate. A wire platinum TE approximately 50 μm in diameter was used for the copper deposition. At a pulse-on time of 400 ns and a voltage of 2 V, copper crystallite islands approximately 60 μm in diameter were obtained. The working electrode potential was maintained near the equilibrium potential of Cu/Cu^{2+} redox system to prevent both large-scale copper deposition and the deposit dissolution.

The method of ultrashort pulses for localization of anodic dissolution was successfully applied to the machining of metals in the active state. For this purpose, the solutions of acids or NaCl are more suitable,

where the passivity range preceding the range of intense active metal dissolution is virtually absent.

ECM of many materials (Ni, Fe, several steels and alloys) in the solutions like NaNO_3 and NaClO_3 proceeds during the anodic dissolution in the state of activation by the salt anions at relatively high polarizations as compared to the active dissolution. In such cases, another mechanism of localization of anodic dissolution by the pulsed current is realized. It requires longer pulses: in addition to EDL charging, a certain charge is required to overcome several stages of metal passivity before the onset of intense metal dissolution [16].

The problem of local anodic dissolution of metals coated with a resistive oxide film (for example, Ti) by ultrashort pulses is that the resistance of such films can significantly exceed the solution resistance. This violates the principle of localization by ultrashort pulses.

Ultrashort pulses are also used in micro-ECM of semiconductors [20]. In this case, the HF-based solutions are commonly used. It is clear that with the localization mechanism described above, the pulse duration will depend on the degree of sample alloying (resistivity) and the gap. The effect of various factors on the results of ECM of semiconductors is complicated by their band structure.

2.3. The Formation of Metal Threads and More Complex Microstructures with a Moving Microdisk Tool-Electrode

The electrochemical formation of metal micro-wires, threads, and columns in many cases is realized using a microdisk TE, which is an end-face of a wire 25–125 μm in diameter embedded into a sleeve of insulating material (Fig. 4) or soldered into glass. During electrodeposition, the microdisk electrode is connected to the positive pole of power source, and the substrate, on which the microstructure is formed, is connected to the negative pole of power source; the microdisk electrode and the substrate are immersed into the solution for metal deposition. In the formation of microstructures by the electrodeposition, insoluble anodes, frequently of Pt, are commonly used. The electrolysis of water with oxygen evolution takes place on these anodes. Sometimes soluble anodes are used. The reduction of cations with the metal deposition, in some cases, with the simultaneous hydrogen evolution, occurs on the cathode.

Prior to the onset of metal electrodeposition, TE is brought at a certain distance to the place on the substrate surface where a metal wire (column) should be grown. Then, a low voltage (for example, 0.1 V) is applied to the electrodes, TE is brought to the substrate until touching, which is recorded by zero electrical resistance or by an abrupt increase of the current. Then, TE is removed to a prescribed distance (frequently by 10 or 20 μm), the operating voltage (several

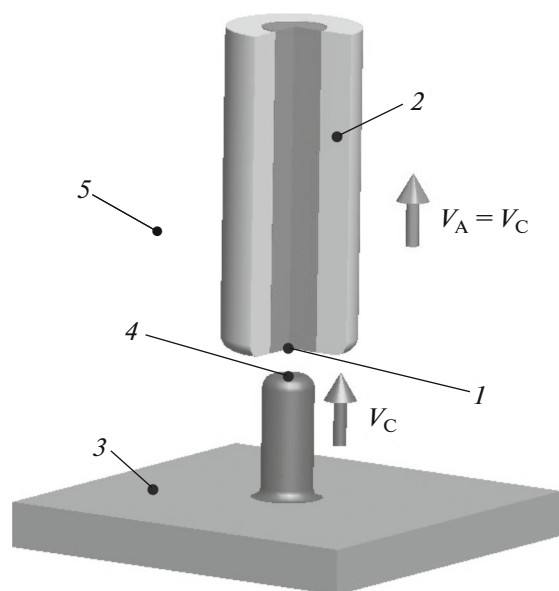


Fig. 4. Scheme of local electrodeposition with continuous anode motion at a constant rate: (1) microelectrode, (2) insulating coating on side surface of microelectrode, (3) substrate, (4) deposit growth surface, and (5) electrolyte.

volts) is imposed, and the metal microwire (thread, column) begins to grow. As a result of the deposit growth, the distance between the anode and the end-face of the formed metal wire decreases. Therefore, to form the deposit with a high aspect ratio, the anode is removed from the substrate at the velocity V_A . Under normal conditions, the velocity V_A should be equal to the deposit growth rate V_C , Fig. 4.

In the mid-90s (20th century), Madden et al. [26, 27]) were the first to develop the method of galvanic formation of microstructures with a large aspect ratio using a moving microanode.

The authors performed the local electrodeposition of nickel from sulfamate electrolyte using various types

of microelectrodes. Two modes of microstructure formation were used. In the first mode, the TE motion was intermittent and controlled by a feedback circuit. When the formed microstructure reached a motionless microelectrode in the course of electrodeposition, the current increased abruptly. This was a signal to remove the microelectrode to a prescribed distance. Then, the next cycle of deposit growth began with motionless TE (Fig. 5).

In another mode, TE moved relatively to the substrate in three-dimensional space along a given trajectory at a constant velocity. In this mode, for example, a 3D part in the form of a spring was formed at a velocity of $6 \mu\text{m/s}$ and nickel microwires $45 \mu\text{m}$ in diameter and up to $1600 \mu\text{m}$ in length were formed.

The method of formation of microwires with intermittent motion of TE has some specific features. Due to multiple contacts of the electrodes and the corresponding high currents, multiply repetition of deposition and TE removal, the formed microwire can have a sinusoidal surface profile, pores and dendrites. The authors of [28–31] proposed the modes of microstructure formation that reduce these difficulties. For this purpose, the contact of the electrodes is not allowed, and TE is removed from WP earlier, when a specified sufficiently high current is reached. In [29], an increase of the current to 20 mA served as the signal for the TE removal. In this case, TE is removed to a predetermined distance or until the desired sufficiently low current is reached, for example [28]. Lin et al. [30], based on the comparative experiments on the local electrodeposition of copper from sulfate electrolyte according to various schemes, propose to remove TE, when the gap decreases by approximately two times. Then, the voltage is reduced to 0.1 V, TE is brought to the contact with the cathode and removed from it to a given distance of $10 \mu\text{m}$. Then, the operating voltage of 3.8 V is imposed and the electrodeposition is repeated.

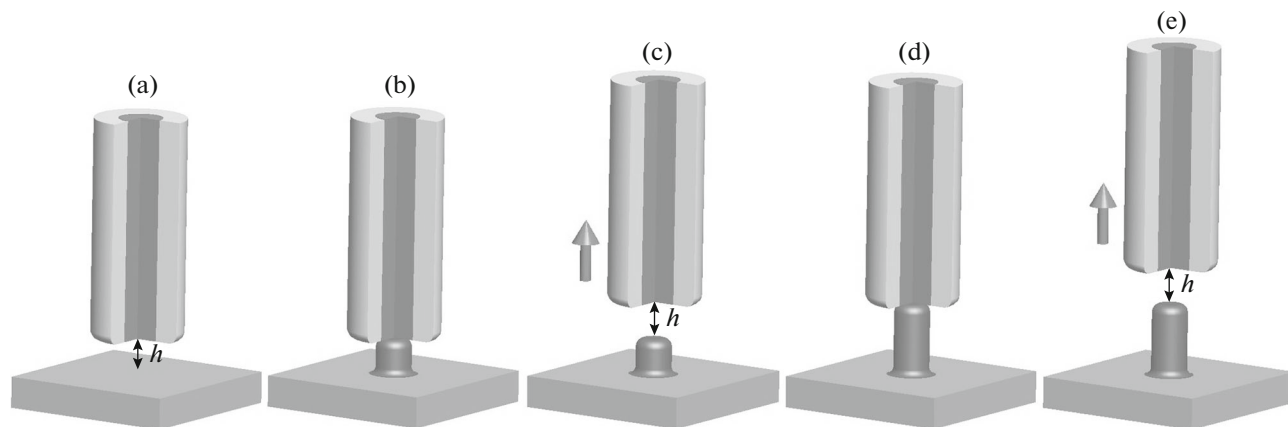


Fig. 5. Scheme of local electrodeposition with intermittent anode motion.

The authors of [32] managed to improve the quality of nickel deposit in the intermittent mode of microwire formation, practically eliminated periodic variation of diameter along the wire length by adding 2–4 mM sodium saccharinate into the electrolyte.

The cyclic process is carried out until a specified wire length is reached. Hundreds and thousands of cycles may be required to complete the work.

In the majority of available works, copper [28, 33–43] and nickel [22, 27, 29, 32, 33, 42] wires were formed, and in some works, the wires of Ni–Cu alloys were formed [37, 44]. Copper [33, 35, 40–43, 45, 46], nickel [42], silver [39, 47], and stainless steel [38] served as the substrates.

In most cases, acidic sulfate electrolyte is used for the copper deposition, and Watts electrolyte, sulfamate electrolyte, and sulfate electrolyte with additives are used for the nickel electrodeposition.

The authors of [41] give an example of important practical application of microthread formation by the local electrodeposition using a moving microdisk electrode: the formation of copper connecting conductor deposited between two contact pads of a microcircuit.

Gas evolution, which can occur both on the insoluble anode and on the cathode during the nickel electrodeposition and during the copper deposition under the conditions of too high potentials, should be taken into account in the analysis of local electrodeposition. On the one hand, the bubble motion generates the electrolyte convection and thus raises the permissible rate of metal electrodeposition. On the other hand, gas bubbles increase the resistance of medium in the interelectrode space.

The proper choice of voltage or cathodic potential is an important factor for controlling the formation of wires, columns and more complex structures by the local cathodic metal deposition.

Wang et al. [39] obtained the dependence of the copper wire deposition rate on the voltage: the deposition rate increases from nearly zero to approximately 26 $\mu\text{m/s}$ with an increase of the voltage from 2.2 to 3.2 V. The dependence is nearly logarithmic.

The average nickel deposition rate increases from 0.078 to 10.06 $\mu\text{m/s}$ with an increase in the voltage from 3.4 to 4.8 V at a gap of 20 μm . The dependence is nonlinear, the deposition rate increases with the voltage steeper than linearly [48].

The quality of the formed microstructure strongly depends on the voltage. The compact cylindrical structure of nickel wire is obtained at a voltage below 3.56 V. The higher is the voltage, the worse is the quality of microwire [45]. The cylindrical copper wire is obtained at low potentials, below 2.4 V, and at an initial gap of 10 μm or smaller. Dendrites and voids in the deposit form at potentials higher than 2.8 V [39].

Along with the voltage, the choice and control of the gap is of great importance. According to [48], the average deposition rate of nickel microwire decreases from 5.4 to 0.33 $\mu\text{m/s}$ with an increase of gap from 20 to 120 μm at a voltage of 4.6 V. In [39], it was shown that the copper wire deposition rate decreases with increasing gap. The rate decreases by approximately 2 times with an increase of the gap by 5 times. The interelectrode distance has an effect on the average wire diameter. The average diameter of copper wire linearly increases from 50 to 130 μm with an increase in the gap from 5 to 30 μm [39]. An intolerable decrease of the gap can lead to a too high current density and reduce the deposit quality.

The structure of the wire from a compact wire to a thin tube depends on the initial interelectrode gap and the voltage [34].

The authors of [48] took into account the importance of the ratio between the voltage and gap; they conducted the experiments at different ratios to form the nickel wires 1500 μm in length. In this work, the best results on the surface quality and deposition rate were obtained at a voltage of 4.6 V and a gap of 80 μm .

A number of works were devoted to various improvements in the methods of forming microstructures.

Hwang et al. [43] used a rotating disk microelectrode to form nickel microcolumns in the mode of intermittent TE motion. The deposition was carried out at a voltage of 4.3 V, a current of approximately 1 mA, and a rotation rate of 1000 rpm. In this case, the current distribution was more uniform, the deposit quality was higher than with stationary TE, the deposition rate was slightly higher, and the reproducibility of results was better. When a rotating TE was used, under certain conditions, not columns, as with a stationary TE, but thin tubes formed on the substrate. The aspect ratio of the tubes reached 16.

In [49], the same authors, instead of TE rotation, imposed ultrasonic oscillations onto the copper substrate with a resonance frequency of 98 kHz of the bath–solution–substrate system. Ultrasonic oscillations reduced the gas filling of the interelectrode space and intensified convective mass transfer in the system. This led to an increase in the thread growth rate, a smaller deviation from the cylindrical shape, an approximation of the column diameter to the TE diameter, and a decrease of the effect of TE surface roughness on the surface quality of the growing deposit. At a higher oscillation frequency (425 kHz), the deposit growth rate increased by 48.6% and the deposit porosity increased by 42.2%.

As a rule, the results of local electrodeposition are better with intermittent motion of TE than with continuous motion, both for the formation of the wires with a high aspect ratio and for the formation of smooth surface and a diameter uniform along the wire length.

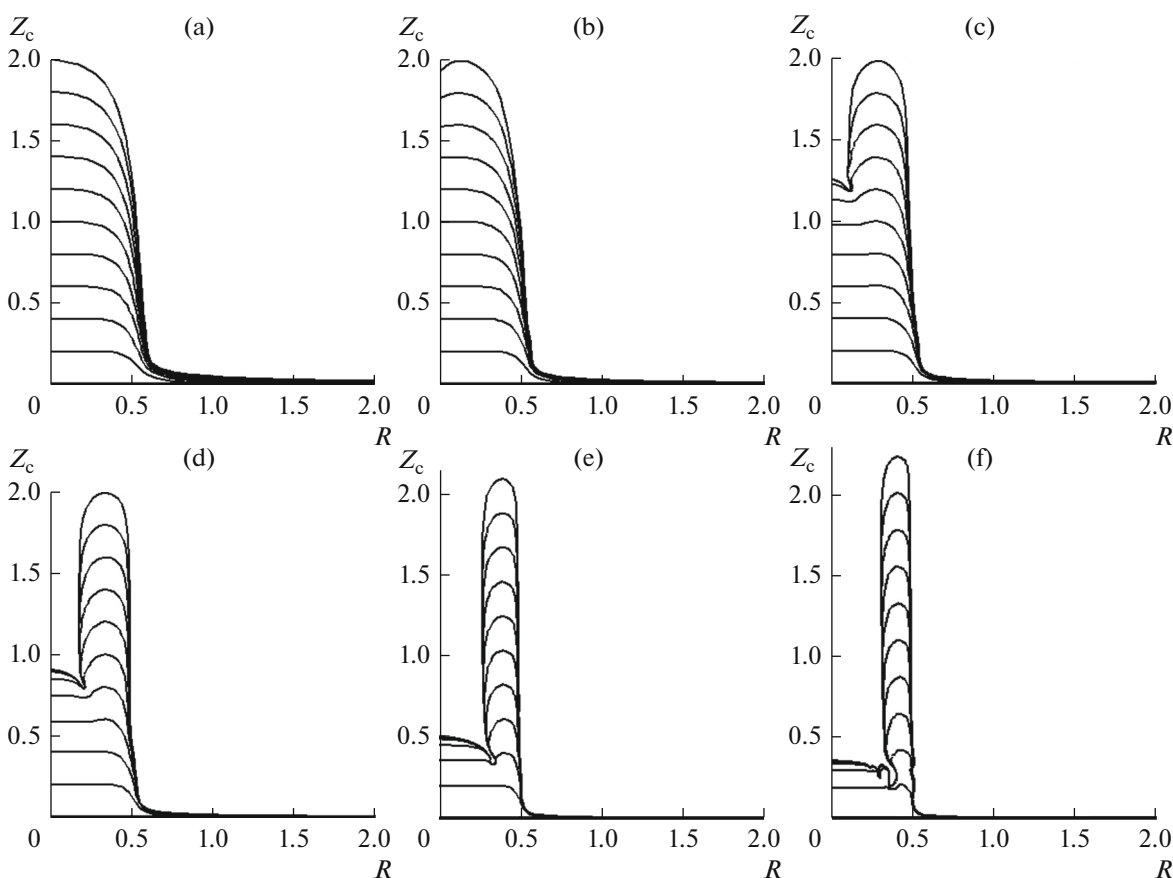


Fig. 6. Evolution of deposit surface during its growth under various deposition conditions with dimensionless time intervals of 0.2 between the lines (0.2, 0.4, ..., 2.0); R is the distance from the axis of symmetry and Z_c is the vertical coordinate; the dimensionless exchange current density increases from Fig. 6a to Fig. 6f.

In a number of works, for example, in [47], it was shown that more complex microstructures, for example, the walls of metal columns located next to each other, can be obtained by the local electrodeposition.

The growth rate and shape of the formed metal thread were analyzed using the methods of mathematical modeling [28, 29, 33, 34, 43, 50–54]. The problems were solved by the methods of boundary and finite elements in the approximation of the primary [16, 29], secondary [51, 55], and tertiary [53, 54] current distribution for cyclic [28, 29, 54] and continuous motion of TE [29, 54].

Depending on the process conditions, the deposits of various morphology can be formed. The deposit shape can vary from cylindrical with different shapes of the upper part to tubular.

Modeling of the process [55] showed that the deposit growth rate and morphology depend on the initial distance between the anode and substrate, the shape and dimensions of the anode and its dielectric coating, the process conditions, and the kinetics of electrode reaction of metal deposition. In this work, the conditions were revealed for the formation of

deposits of various types, including cylindrical deposits with various shapes of the end-face, the metal thread, and tubular deposits, Fig. 6. For instance, cylindrical deposits with a flat end-face form at small initial interelectrode distances and a low exchange current density of electrochemical reaction. Under the conditions of small initial gaps and a high exchange current density of electrochemical reaction, tubular deposits can form due to a strong edge effect.

The above-described method of electrochemical formation of microstructures does not enable one to obtain the nanoscale structures on the substrate surface, as is achieved, for example, using scanning microscopes. However, it enables the formation of microstructures with a very high aspect ratio up to 1 : 282 [36].

2.4. Application of Scanning Probe Microscopes (SPM)

The progress in SPM and the development of scanning electrochemical microscopy led to the application of SPM for the formation of metal micro/nanostructures and surface modification by the local electrodepo-

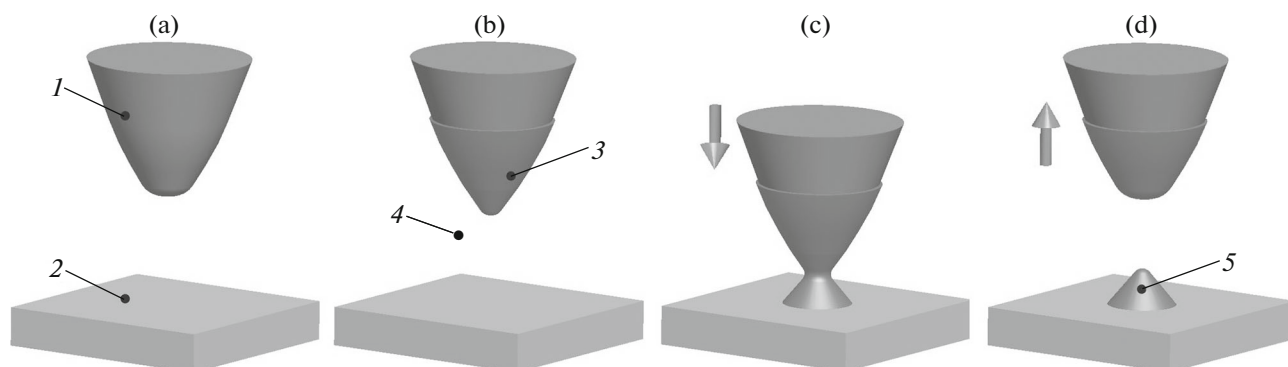


Fig. 7. Scheme of local electrodeposition using insoluble anode: (1) anode, (2) substrate, (3) metal layer deposited on anode, which was temporarily used as the cathode, (4) electrolyte solution containing metal ions, and (5) micro/nano cluster of metal on substrate surface.

sition or etching of metals and semiconductors. For this purpose, various types of probe microscopes (tunnel, force, and electrochemical microscopes) are used after the necessary modification. The modified SPM devices have turned into technological tools for the formation of various nano/microstructures for nanoelectronics, nanosystem engineering, and microelectromechanical devices. A specific feature of application of SPM for these purposes is that both the probe and substrate are located in an electrochemical cell filled with an electrolyte solution.

In the local ECM with the use of SPM, as a rule, a metal or metallized microscope probe, which is coated with chemically resistant dielectric material except for a tip of nano- or micro-dimensions, serves as the tool-electrode. The etching or deposition of metal occurs locally immediately under the uninsulated probe tip with a gap of the same order of magnitude as the probe tip dimension.

In the direct ECM method, for example, etching, the probe tip serves as the cathode. Under certain conditions, a metal deposit can form on the cathode and gas bubbles can evolve. This can change the geometry of probe tip and reduce the accuracy of micro-ECM. In addition, in this case, the substrate potential is more positive; this can lead to the substrate corrosion, the oxide formation.

The indirect processes of local metal electrodeposition or dissolution using SPM in the feedback mode, when electron transfer on the substrate determines the current on the microelectrode, are widely used.

Micro-ECM with SPM in the feedback mode is performed in the four-electrode electrochemical cell: commonly, a Pt microelectrode (TE), Pt auxiliary electrode, a reference electrode, and a substrate (WP), which is not connected to an external power source. The potentials of microelectrode and auxiliary electrode against the reference electrode are controlled by a bipotentiostat. The substrate potential is reached under the action of the redox system in the cell.

At a sufficiently large distance between the microelectrode and substrate (several diameters of the microelectrode), the current between the microelectrode and auxiliary electrode is low. As the microelectrode approaches the substrate, a fraction of the reaction product on the microelectrode manages to reach the substrate due to diffusion and enter into the reaction there.

A relatively high current arises between the microelectrode and the substrate; the smaller is the distance between them, the higher is the current (positive feedback).

If the reaction product on the microelectrode cannot react on the substrate for some reason, the substrate only hampers the access of the reagent to the microelectrode; the smaller is the probe–substrate distance, the lower is the current in the system. This is the negative feedback mode. The known relationship between the current and distance, both with positive and negative feedback, enables one to control the distance between the probe and substrate, which is necessary for micro/nano ECM.

The micro-ECM in the feedback mode is frequently used in the processes described in section 4.3.

2.4.1. Electrodeposition of metal on a probe with subsequent local redeposition on a substrate. The Kolb's group [56–60] developed a technique for decorating a substrate with metal clusters; it was called “a jump to contact”. First, a potential, at which a metal, for example, copper, is cathodically deposited from the solution on the probe surface, is imposed onto the probe, Fig. 7a. (The desired potential is set against the potential of Cu/Cu²⁺ redox pair using a bipotentiostat). Then, the probe with the deposited metal is brought for a short time so close (0.8 ± 0.2 nm) to the substrate that a bridge of the metal (Fig. 7b) deposited on the probe is formed between the probe and substrate, Fig. 7c. The bridge breaks in the subsequent removal of probe from the substrate and leaves a metal cluster on the substrate, Fig. 7d. The process is carried

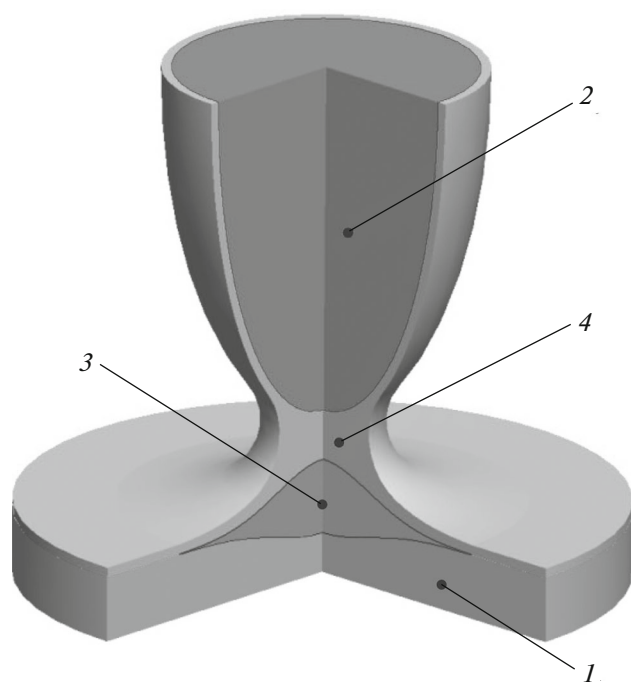


Fig. 8. Scheme of local oxidation through water meniscus: (1) anode, (2) cathode, (3) metal oxide, and (4) meniscus.

out in the pulsed mode with a pulse duration of 10–20 ms and a frequency of 50–80 Hz.

The convergence and removal of the electrodes with simultaneous substrate motion enabled one to form large masses of individual metal clusters on the substrate. A completely automated process was developed for this purpose [58].

According to [58], copper clusters with an average height of 0.7 nm were formed on the Au substrate in the 0.05 M H_2SO_4 + 0.1 mM CuSO_4 solution at a rate of 50 clusters per second, the distance between the clusters was 11 nm. The formation of 10000 clusters took 17 min. A certain change in the geometry of probe tip due to the transition of copper from the tip to the substrate can have a small effect on the distance between the clusters.

The average cluster height is 0.2–1.5 nm. The height of clusters is affected, in particular, by the distance between the probe and substrate. High stability of clusters, which is observed in some cases, is explained by the alloy formation.

The formation of large arrays of palladium nano-clusters is of great interest from the viewpoint of developing effective catalysts. In [61], the formation of 400 palladium clusters with an average height of 0.4 nm on the area of 190×190 nm at a rate of 80 clusters per second was demonstrated in the 0.05 M H_2SO_4 + 0.1 mM H_2PdCl_4 solution in the completely automated process.

Hofmann, Schindler et al. [62–64] performed local deposition of magnetic cobalt clusters onto Au substrate with intermediate deposition onto the probe and redeposition onto the substrate in the two-step process, which differs from the Kolb work by the absence of any contacts between the probe and substrate.

2.4.2. Metal deposition on the semiconductor substrate. SPMs are used for the micromachining of semiconductors. The majority of the published works are devoted to the electrodeposition of metals on the *n*-semiconductors, and a smaller number of works are devoted to the deposition on the *p*-semiconductors. The reason is that the *n*-semiconductors behave “like conductors” under the cathodic polarization. An electrochemical reaction on the *p*-semiconductor can proceed only at a sufficiently large potential shift from the open-circuit potential, in the potential range above the potential, which is commonly attributed to the breakdown of the Schottky blocking barrier [65]. The breakdown potential can be significantly reduced by the preliminary local activation in the areas intended for deposition. Therefore, such a pretreatment of substrate is important especially for the electrodeposition of metals on the *p*-semiconductors.

The mechanical activation is most frequently used. It is carried out using a SPM with a diamond probe smaller than 25 nm in radius. The probe is pressed into the surface layer of semiconductor and forms the defects on the area in the shape of a scratch. The defective areas in the shape of a circular cavity can be formed by the directed jet of a liquid with SiO_2 particles. As a result of local mechanical activation of semiconductor surface, spontaneous metal deposition can occur without an external power source due to a potential difference between the activated and passive, non-activated areas of substrate surface [66, 67]. The effectiveness of this method was shown by the authors of [66] by the example of local copper deposition on *p*-Si(100) in the mixture of HF and $\text{Cu}(\text{NO}_3)_2$: $2\text{Cu}^{2+} + \text{Si} + 6\text{HF} = \text{H}_2\text{SiF}_6 + 2\text{Cu} + 4\text{H}^+$. The nanostructures with the characteristic dimensions of 50 nm were formed.

The local micro/nano-electrodeposition of metals on the semiconductor substrates was studied in [67–71] and other works.

The problems of thermodynamics and kinetics of metal electrodeposition on Si, and, especially, the analysis of the results of Cu, Au, and Pt deposition are reviewed by Oskam et al. [72].

2.4.3. Local oxidation of metals and semiconductors. In the humid air atmosphere, a drop of water, meniscus forms between the sharp tip of the SPM probe and the substrate, and the oxidation is performed through the meniscus, Fig. 8. TE is connected to the negative pole of power source, and a metal or semiconductor substrate (commonly film) is connected to the positive pole. The process is carried out

at a given voltage, a given current, or in a pulsed mode. As well as in other versions of local ECM, the probe and substrate can move in various directions. This enables one to form oxide “spots” or “lines”, strips on the workpiece surface.

The oxidation has the same nature as in the conventional electrochemical oxidation:



The reduction of oxygen dissolved in water $O_2 + 4e + 2H_2O \rightarrow 4OH^-$ or, at the sufficiently high potentials, the water electrolysis $4H_2O + 4e \rightarrow 2H_2 + 4OH^-$ proceeds on the cathode (probe).

The key parameters for controlling local oxidation are the probe shape and dimensions, the voltage between the electrodes, the current in the galvanostatic mode or the parameters of the pulsed mode, the process duration for the formation of “spots” or the probe scan rate for the formation of oxide lines, and the air humidity [73–80].

The operating voltage is several volts (2–10 V, sometimes up to 25 V). The probe scan rate ranges from 0.01 to 10 $\mu\text{m/s}$ depending, in particular, on the line length (the longer is the line, the higher is the scan rate). When the “spots” are formed, the oxide thickness (in a certain range) increases almost linearly with increasing voltage and pulse duration. When the lines are formed, the oxide thickness depends logarithmically on the scan rate, the line width and oxide thickness increase linearly with the applied voltage. As well as in the conventional electrochemical oxidation, the Pilling–Bedworth ratio (the ratio between the volumetric electrochemical equivalents of the metal and its oxide), which depends on the metal nature, is an important characteristic of the process. The strip width and oxide thickness (or the height of oxide line above the WP surface) decrease with increasing scan rate and increase (within certain limits) with increasing voltage. The strip is 20–100 nm in width. The strip width and the aspect ratio (the ratio of oxide height to strip width) depend on the relative environmental humidity. For example, in [73], it was found that in the oxidation of *n*-type Si at a scan rate of 300 nm/s, at a relative humidity of 14%, the oxide line 23 nm in width was obtained; this is approximately 4 times smaller than at a humidity of 61%, and the aspect ratio was significantly higher.

The method of local electrochemical oxidation was used for machining aluminum [81], silicon [79, 82, 83], titanium [84, 85], tantalum [77], vanadium [76], chromium [86], and other materials.

In [74], the local oxidation of silicon and metals was reviewed, and the kinetics and mechanism of the processes were discussed.

3. ELECTROCHEMICAL DEPOSITION AND DISSOLUTION USING TOOL-ELECTRODE IN MICRO/NANOPIPETTES AND NOZZLES

3.1. Formation of Microstructures with Moving Microelectrode in Free Pipette through Liquid Meniscus

Along with the microelectrode shown in Fig. 5, another type of moving microelectrodes is used to form the microstructures with a high aspect ratio (the microwires and metal threads). This is a glass micropipette filled with a solution for metal electrodeposition with the anode inside it. The process is carried out without immersing the electrodes into a bath with an electrolyte, in the air environment with some relative humidity. When the pipette touches or almost touches the substrate, an electrolyte meniscus, a liquid bridge between the micropipette tip and the substrate, forms. When this tool is used, the active zone of the substrate is limited by the meniscus, Fig. 9.

The electrolysis is performed by the two-electrode scheme or by the three-electrode scheme using a potentiostat.

When the voltage is imposed, the current abruptly increases. Then, the pipette is removed to the required distance, at which the steady-state current is reached and the wire grows. As the wire grows, the pipette should be removed from the growing surface at a certain rate, Fig. 9a. The meniscus diameter and height are of the same order of magnitude as the diameter of pipette tip.

In this process, the water evaporation from the meniscus surface is the most important factor; it is considerable due to a high ratio of the meniscus surface area to its volume. The humidity of the environment, where the electrodeposition is carried out, has a pronounced effect on the evaporation.

The evaporation causes convection with the delivery of liquid from the micropipette to the meniscus.

The loss of water due to evaporation through the meniscus surface generates a convective flow of Cu^{2+} ions in the meniscus and, thus, significantly affects the ion distribution [87]. The water evaporation occurs at the meniscus–air interface; therefore, the metal growth rate is higher here. A difference in the microwire growth rate arises in the radial direction in its cross section, and the microwire growth front becomes not flat. This is especially noticeable at a relatively low environmental humidity [88]. To obtain a compact cylindrical structure, it is necessary to eliminate the difference between the metal deposition rates in the peripheral and central zones [87]. Conversely, the favorable conditions for reaching a large difference between these rates enable one to form microtubes rather than wires.

The pipette can be shifted to the right or left by several micrometers without breaking the meniscus; this can be used to form various 3D microstructures, Fig. 9b.

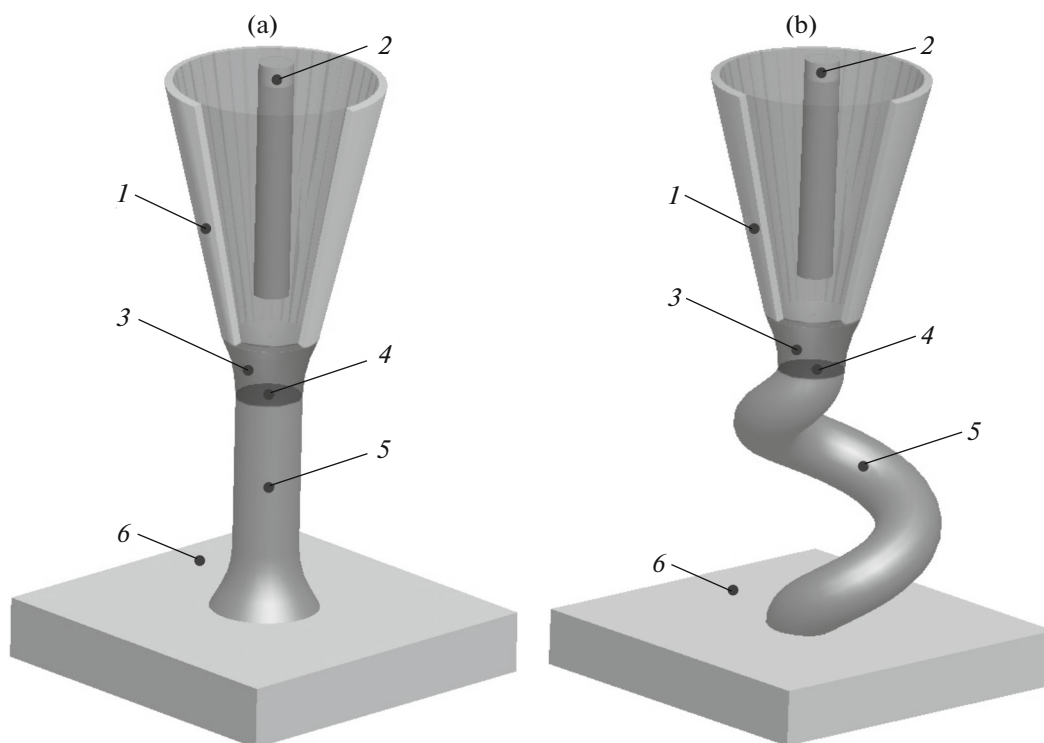


Fig. 9. Schemes of local metal electrodeposition through meniscus in humid air: (1) micropipette with electrolyte solution, (2) anode, (3) meniscus, (4) deposit growth front, (5) growing microstructure, and (6) substrate (cathode).

It is clear that environmental humidity control is important. The optimal value of relative humidity is 60–80% and depends on many factors [38]. Other works were performed at a humidity of 50% [87, 89].

The higher is the humidity, the lower are the evaporation rate and the microwire growth rate. At too low humidity, the crystallization of a salt, for example, CuSO_4 , can occur near the pipette tip and the metal deposition can be disturbed. The use of CuSO_4 of too high concentration in an attempt to raise metal deposition rate can lead to the same result.

The diameter of the hole in the micropipette is of great importance. In various works, the hole is from 100 nm to several micrometers in diameter. An increase of diameter leads to an increase of the current and a decrease of the evaporation rate of water in the meniscus [90]. The deposition rate decreases with increasing hole diameter within certain limits. At different diameters of holes in the pipette, the copper deposition rate is 0.18 $\mu\text{m/s}$ (20.4 $\mu\text{m}^3/\text{s}$) [87], from 520 nm/s to 2.3 $\mu\text{m/s}$ and from 15 nm/s to 45 nm/s [91], 88 nm/s and 263 nm/s [90], 0.25 $\mu\text{m/s}$ [92], 0.008 $\mu\text{m}^3/\text{s}$ [89], and from 100 nm/s to 0.18 $\mu\text{m/s}$.

There is a certain range of tolerable rates of micropipette removal from the growing wire [90]; beyond this range, the meniscus becomes unstable and breaks. The shape of meniscus depends on the micropipette rate. Within the range of tolerable rates, the wire diameter decreases with increasing rate. For example, at a diameter of hole in the micropipette of 730 nm, an

increase in the rate from 88 nm/s (the lowest tolerable rate) to 263 nm/s (the highest tolerable rate) leads to a decrease in the wire diameter from 657 to 365 nm.

The authors of [92] showed that the micropipette removal rate can be used to control the wire thickness by narrowing the meniscus with increasing rate. Using a pipette 1.6 μm in diameter and the pipette removal rate of 0.25 to 0.4 $\mu\text{m/s}$, a wire 1400 to 1100 nm in diameter was deposited.

In the work of Seol et al. [87], not only rectilinear fragments of microwires, but also more complex structures were grown.

The authors of [92] showed that the micropipette retraction rate can be used to control the thickness of the wire, narrowing the meniscus with increasing speed. They used a pipette with a diameter of 1.6 μm and a pipette removal rate from 0.25 to 0.4 $\mu\text{m/s}$ and deposited a wire with a diameter of 1400 to 1100 nm.

In the work of Seol et al. [87] not only rectilinear fragments of microwires were grown, but also more complex structures.

The authors of [92] solved a similar problem by developing a micropipette with a special tip shape. In addition, the micropipette trajectory was varied. As a result, the microwire can be bent during its growth and oriented in the direction from 0° (parallel to the substrate surface) to 90° (normal to the substrate surface). Figure 10a shows the micropipette tip and a series of copper wires formed by this micropipette at different angles. Figure 10b shows the examples of the application of this method for grow-

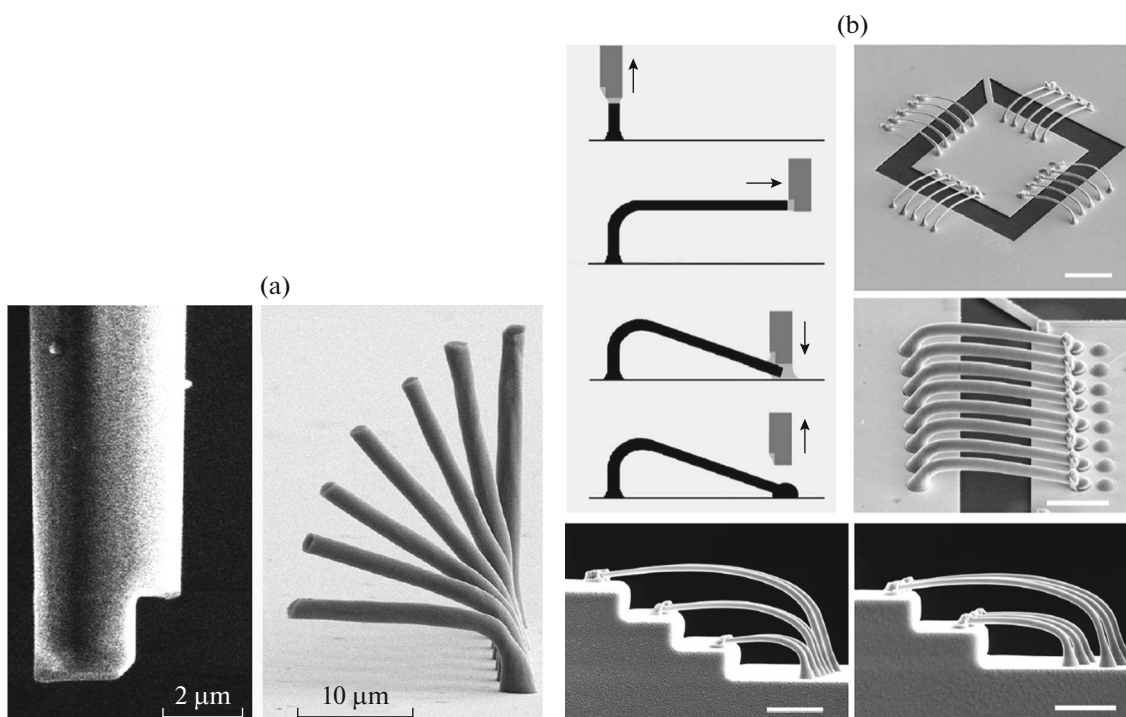


Fig. 10. (a) Modified tip of nanopipette and illustration of results of its application to form nanowires with different angles of inclination. (b) Scheme of formation of microwires for electrical contacts of chips [92].

ing copper wires 740 nm in diameter and 40 μm in length. These are the electrical contacts of chips (the scale mark in Fig. 10b is 10 μm in length).

In [89], it was shown that thin platinum nanowires 150 nm in diameter with an aspect ratio of 200 can be formed.

Copper microwires 200 nm in diameter and 10 μm in length were formed in the 0.05 M CuSO_4 solution [91]. By way of example, the formation of a complex of 100 nanowires spaced at intervals of 7 μm was described. Stable copper deposition was carried out at a pipette removal rate of 250 nm/s. The process was totally automated.

In the majority of works, where the nanopipettes are used, the copper deposition rates are low, from 100 nm/s to 0.18 $\mu\text{m}/\text{s}$ (0.008–20.4 $\mu\text{m}^3/\text{s}$). A new approach proposed in [93] extends the capabilities of the method. A syringe with a significantly larger hole 400 μm in diameter is used. An open-pore sponge soaked with a solution for copper deposition is placed into the conical part of the syringe. This part of device is the writing head of electrochemical 3D printer. The sponge prevents the free flow of the solution out through a large hole in the syringe and thus provides the formation of stable meniscus. In addition to 1 M CuSO_4 solution, copper plates, which are used as the auxiliary electrode and reference electrode, are placed in the syringe. When the writing head moves along the substrate surface at a rate of 0.4 mm/s, a convex pattern of a given shape is formed. The strip width is from 3 to 15 μm depending on the potential (1–4 V against

the copper electrode). A strip 10 mm long with a layer thickness of 14–104 nm is formed in one hour of operation. This requires 144 head passes. The method enables one to achieve a copper deposition rate of 19667 $\mu\text{m}^3/\text{s}$ with no dendrite formation.

3.2. Formation of Metal Microstructures with Moving Microelectrode in Pipette Immersed into Electrolyte

The micropipettes shown in Fig. 9 can be used for local ECM when immersed into the solution. The advantage of this technique is the absence of the problem of meniscus stabilization. The drawback of this technique is the current dissipation in the electrolyte; as a result, the metal deposition occurs not only directly under the hole in the pipette, but also on the adjacent substrate areas. The wire thickness is substantially larger than the diameter of pipette hole.

Momotenko et al. [94] used a nanopipette with a hole 30–50 nm in diameter divided lengthwise into two parts. The current of copper column deposition flows through one part of the pipette. Concurrently, through another pipette part, using the feedback circuit, the distance between the nanopipette and the substrate surface is controlled during the formation of nanowire segments of various shapes.

In the above example, the nanowires are 500 nm thick and several micrometers in height.

In some works, the pipette with the electrolyte was a part of the SPM cantilever.

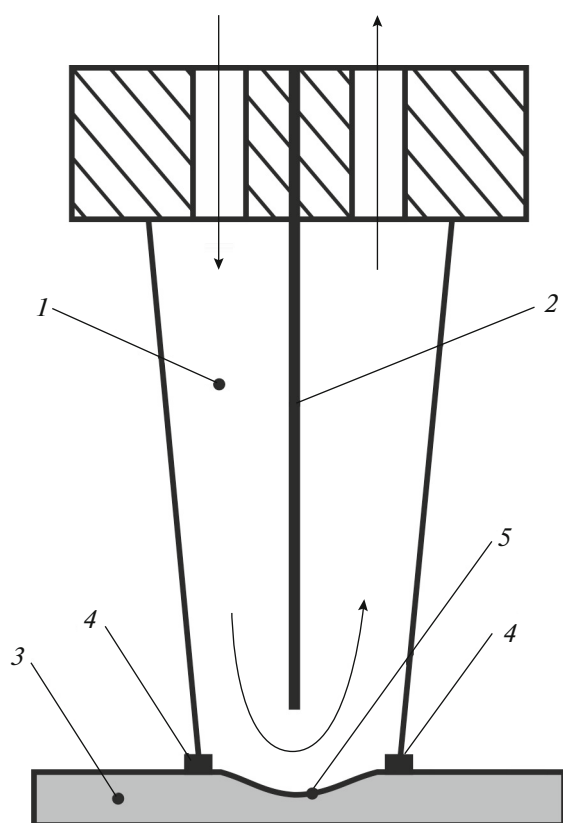


Fig. 11. Scheme of microcell: (1) capillary, (2) partition, (3) substrate, (4) seal, (5) cavity formed at the initial stage of the electrochemical “drilling” of hole. The direction of solution flow is shown with arrows.

3.3. Metal Electrodeposition Using SPM with a Probe in the Form of Micropipette with Electrolyte

Muller et al. [95], probably, were the first to develop a setup for the local metal electrodeposition containing a scanning probe microscope with a micropipette as a probe and a bipotentiostat.

Ito and Iwata [96] replaced a probe of SPM by a nanopipette with an anode (copper wire 30 μm in diameter) and a solution for local copper electrodeposition on the gold substrate. They used two versions: the pipette tip is located at some distance from the substrate surface (the island diameter is considerably larger than the pipette hole diameter) or the pipette tip is practically in contact with the substrate (the island diameter is close to the hole diameter).

The hole in the glass pipette was 200 nm in diameter, and the outer diameter of the pipette tip was 300 nm. Copper was deposited from 0.001 M CuSO_4 solution. The pipette tip and substrate were placed into the solution in the electrochemical cell. This prevented the solution in the pipette from drying and clogging the hole. To control the distance between the pipette tip and the substrate, the pipette was con-

nected to a quartz resonator and oscillated in the vertical direction. The pipette oscillated with an amplitude of less than 10 nm at a resonant frequency depending on the distance between the pipette tip and the substrate. The distance was maintained constant by varying the resonance frequency as the pipette approached the substrate.

The method used to control the distance between the pipette tip and the substrate enabled one to carry out the process at almost zero distance and to obtain a metal island on the substrate of almost the same dimension as the pipette hole diameter. The islands of highly reproducible dimensions were obtained.

The deposition of one island 198 nm in diameter and 28 nm in height at a voltage of 3.5 V took 2.5 s.

The authors of [97] used a set of 10 silicon micropipettes with the inner surface coated with gold (anodes) as the microcantilevers. The channels in the pipettes were filled with the electrolyte for electrodeposition of copper islands on the Au substrate that served as the cathode. The electrolyte drops were applied to the substrate from each cantilever to those places where the copper islands should be formed using the direct contact of cantilever tip with the substrate. The dimension of the hole in the cantilever was $4 \times 5 \mu\text{m}$. The distance between the electrodes was 6 μm . The drops were several tens μm in diameter. The copper island dimension depended on the duration of voltage pulse, it was commonly 20 μm .

3.4. Application of Electrochemical Microcells for Local ECM of Metals

By the electrochemical microcell in the micromachining is meant a capillary with an electrolyte and a counter electrode pressed against WP with a seal around the periphery of the capillary tip, which prevents the electrolyte from leaving the connection of capillary with the workpiece. Such a cell was used for the first time back in [98] for local anodic dissolution of metal.

To raise the ECM rate, the process is conducted in the electrolyte flow. For this purpose, the capillary is divided along the axis into two parts by a glass partition. The partition does not reach the capillary tip, so that a space remains between the lower end of partition and the substrate. This allows electrolyte to flow to the substrate on one side of partition and from the substrate on the other side of partition [99]. A small hole diameter (about 10 μm) and intense electrolyte flow in the capillary enable one to obtain high current densities (up to 100 A/cm^2) at low currents.

It should be noted that a similar technique was used at the very beginning of the 20th century for electrochemical drilling of holes in armored steel in the sulfuric acid solutions [100, 101], Fig. 11. Unfortunately, this work is almost forgotten now.

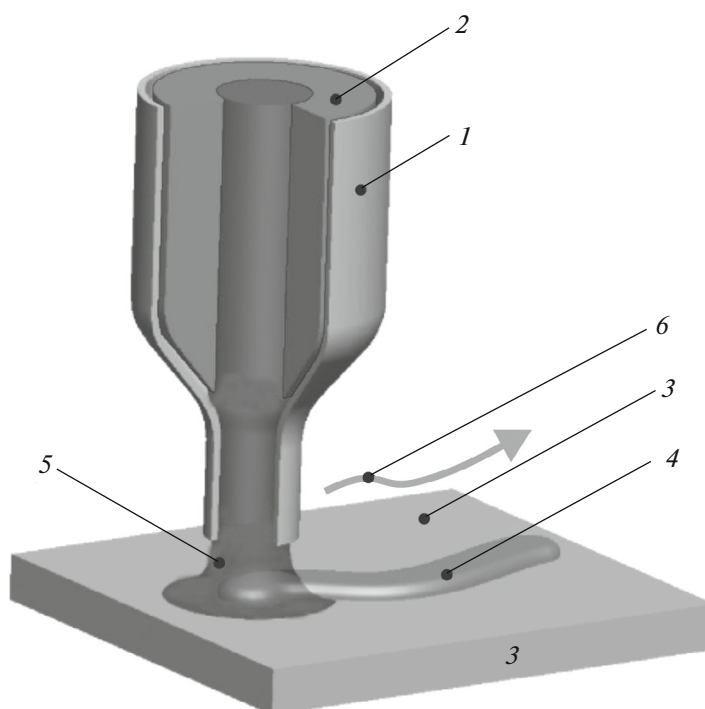


Fig. 12. Device for jet metal electrodeposition: (1) glass nozzle, (2) anode, (3) substrate, (4) “path” of deposited metal, (5) meniscus, and (6) arrow shows the direction of substrate motion.

3.5. Jet Electrochemical Micromachining

Jet electrochemical machining (JECM) is a method of local electrochemical metal dissolution or deposition, when a free electrolyte jet from a nozzle under a pressure is directed to the WP surface area, where the electrochemical machining should be performed.

In the case of metal dissolution, the nozzle can be made of metal and serve as the cathode (in some cases, there is a glass tube inside the metal nozzle through which the electrolyte is supplied). In the electrodeposition, the nozzle is commonly made of glass, and the metal insoluble anode is placed inside the nozzle, Fig. 12.

This method enables the formation of individual islands of electrodeposited metal or micron-scale cavities. Using scanning of WP surface, convex or recessed pattern lines can be formed according to a given program.

The machining is controlled by choosing the composition, concentration, and temperature of the electrolyte, voltage or pulsed current parameters, nozzle diameter, distance from the nozzle to the WP surface, the rate of the nozzle or WP during the dissolution or deposition of lines, and the process duration. In the case of metal dissolution, NaNO_3 or NaCl solutions are commonly used as the electrolyte. The distance between the nozzle tip and the WP surface is from several tens of μm to several mm. The nozzle diameter

varies within the same range. The voltage varies from 5 to 100 volts and higher. The voltage is higher when a glass nozzle with an electrode inside it is used due to a larger interelectrode gap. The diameter of the resulting cavity or deposited island and the width of the strip formed by moving the table with WP are approximately 2 times larger than the electrolyte jet diameter.

A large series of work on the jet electrochemical drilling began mainly in the 60s in connection with the development of electrochemical machining and continues to the present. In recent years, a direction related to micro-ECM has been developed; it is presented as an “electrochemical printing”, for example [102].

In JECM, very high current densities are reached: up to several tens A/cm^2 in the electrodeposition and up to several hundred A/cm^2 in the anodic dissolution due to a small gap and the electrolyte flow. This enables one to obtain not only a high productivity, but also a high surface finish (low roughness). It was repeatedly indicated that the surface roughness decreases with increasing current density in the anodic dissolution of metals. In [103], it was shown that during jet ECM, at the current densities of about $150 \text{ A}/\text{cm}^2$, various metals (iron, stainless steel, copper, and aluminum) are polished in the aqueous solutions of salts (KNO_3 and KCl). In [104], it was shown that very high current densities, up to $300 \text{ A}/\text{cm}^2$, which can be reached in JECM, enable one to reduce or

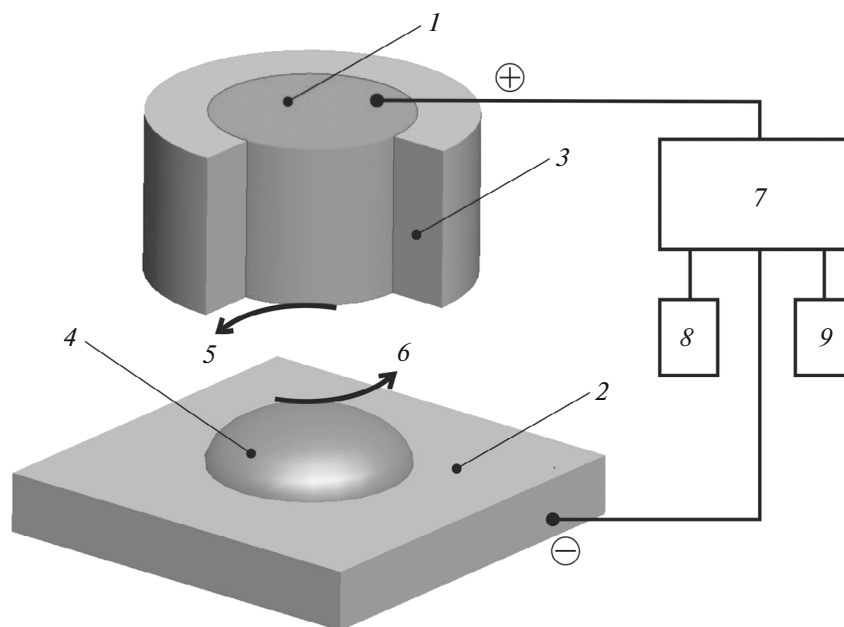


Fig. 13. Scheme of local electrodeposition using insoluble microelectrode: (1) microelectrode/anode (Au, Co), (2) conducting substrate, (3) dielectric coating on anode, (4) microisland of deposited metal, (5) metal complex with activating anion (AuBr_4^- , CoCl_x^{2-x}) formed by the dissolution of anode, (6) activating anion (Br , Cl^-) formed in metal deposition on the cathode, (7) bipotentiostat, (8) reference electrode, and (9) auxiliary electrode. Reference electrode and auxiliary electrode are located in the solution together with the microelectrode and substrate. Four-electrode scheme.

eliminate the effect of preliminary mechanical or heat treatment of WP on the surface quality after ECM.

The studies lead to the conclusion that the best results can be obtained using the independent control of the current density and hydrodynamic parameters [102].

The capabilities of the method with respect to the shape of the formed cavity and the surface finish can be extended by using the electrolyte jet directed at a given angle to the WP surface and by rotating the jet relative to the direction of tool motion [105, 106].

Natsu et al. [107, 108] developed a method for fabricating three-dimensional cavities using the anodic dissolution of metals by the JECM method. In the setup for this method, the nozzle can move not only normally to the WP surface; the axis of symmetry of the nozzle can also move around a circle. In one version of the method, the nozzle moves against the WP surface and stops for a short time in the places, where the cavities should be formed. The cavities can be arranged in the desired order and form the WP surface (plane or cylindrical) occupied with a system of cavities. In another version of the method, the nozzle does not stop to form a cavity on the WP surface, but moves at a given rate over certain distances to form a system of long cavities, tracks. A setup for JECM is controlled by a computer so that the superposition of individual tracks forms a three-dimensional cavity very close to the desired shape.

JECM is used for the local oxidation of aluminum [109, 110].

4. LOCALIZATION OF ELECTROACTIVE COMPONENT OF ELECTROLYTE IN THE MACHINING ZONE

In this approach to the organization of micro/nano-ECM, the reagent for the local deposition or dissolution of the metal (semiconductor) on the substrate is not contained in the bulk electrolyte, but forms on the microelectrode, which is placed at a very small distance from the substrate, or in another way. The process localization is provided both by localizing the electric field and by localizing the source of the reagent in close proximity to the place of deposition or dissolution on the substrate. There are several versions of this approach to micro/nano-ECM.

4.1. Local Electrodeposition of Metal with Soluble Anode

The local electrodeposition of gold and cobalt can serve as the examples [111, 112]. A microscope probe of several tens micrometers in dimension serves as the soluble microelectrode (TE); it is made of the same metal that should be deposited on the substrate, Fig. 13.

In [111], the local electrodeposition of gold is performed from the 0.1 M HBr solution on the ITO substrate. The required potentials of TE and substrate are set using a bipotentiostat. The gold dissolution proceeds by reaction $\text{Au} + 4\text{Br}^- \rightarrow \text{AuBr}_4^- + 3\text{e}^-$. The resulting compound diffuses to the substrate and is reduced with the formation of a metal island on the substrate and Br^- anions, which diffuse to TE and again participate in the gold dissolution. The smaller is the gap, the higher is the current (a positive feedback). This process enables one, for example, to apply the required gold pattern onto a conductive substrate ("gold pen"). The resolution of the process depends on the dimensions of the microanode and gap.

The local electrodeposition of cobalt is performed with a soluble microelectrode (probe of SPM) 50 μm in diameter using a somewhat more complicated procedure associated with the formation of an oxide film on the anode, which hampers the deposition [112].

4.2. Local Electrodeposition of Metal. SPM with Insoluble Probe Microelectrode. Method of Chemical Lenses

In order to enhance the lateral resolution of local metal electrodeposition using SPM, the authors of [113, 114] proposed the method of chemical lenses. In the local electrodeposition of silver on the gold substrate, a probe, the end-face of platinum wire 10 μm in diameter, serves as a microelectrode. The solution contains AgNO_3 , ammonia to form a complex with silver $[\text{Ag}(\text{NH}_3)_2]^+$, NaNO_2 , and NaNO_3 (the latter is used to ensure sufficient conductivity). A bipotentiostat is used for imposing independently the required potentials onto the microelectrode and substrate. On the microelectrode, the oxidation proceeds: $\text{NO}_2^- + \text{H}_2\text{O} \rightarrow \text{NO}_3^- + 2\text{H}^+ + 2\text{e}^-$. Formed H^+ ions shift the equilibrium $[\text{Ag}(\text{NH}_3)_2]^+ + 2\text{H}^+ \leftrightarrow \text{Ag}^+ + 2\text{NH}_4^+$ in the solution in the direction of formation of Ag^+ cations; a fraction of these cations manage to diffuse to the substrate and are reduced to Ag. Those Ag^+ cations, which diffuse from the microelectrode not along the shortest path, more likely, react with ammonia to form an inactive complex with respect to the reaction on the substrate at its given potential. Thus, a channel, a lens forms between the microelectrode and the substrate (Fig. 14), inside which Ag^+ are present. The presence of complexing agent limits the lateral dimensions of lens and assists the localization of electrodeposition.

4.3. Local Etching of Metals and Semiconductors in the Positive Feedback Mode

The etching of metals and semiconductors is carried out in the positive feedback mode of SPM, see

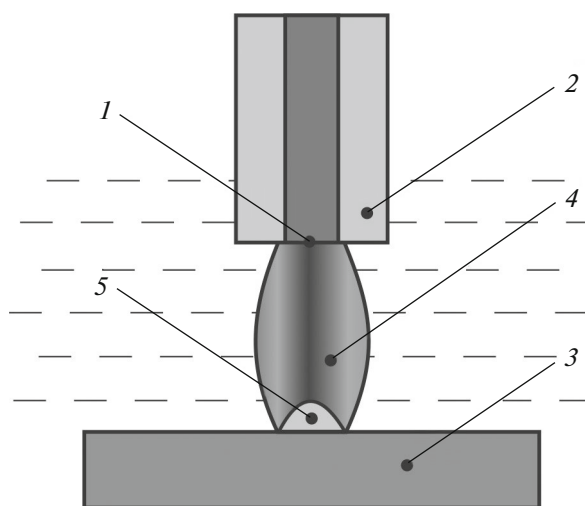


Fig. 14. Scheme of local electrodeposition using chemical lenses: (1) microelectrode, (2) insulation of side surface of microelectrode, (3) substrate, (4) chemical lens, and (5) micro-island of deposited metal.

section 4.1. In this method, the etchant is not contained in the electrochemical cell, but forms on the microelectrode as a result of oxidation of the reduced form of redox system. At a sufficiently small distance between the microelectrode and substrate, the formed oxidized form (etchant) realizes local etching of the substrate directly under the microelectrode and is converted into the reduced form, which diffuses to the microelectrode and undergoes oxidation again, Fig. 15.

For instance, in the local etching of semiconductors, for example GaAs, the mixture of 0.02 M HBr and 0.5 M HCl serves as the redox pair. Anions Br^- are oxidized on the Pt microelectrode with the formation of strong oxidant Br_2 , which diffuses to the substrate and oxidizes (dissolves) GaAs, whereas Br_2 is reduced to Br^- , which is oxidized on the microelectrode to Br_2 , and so on [115, 116].

This method was also used for the local etching of copper films, but with other redox pairs: $\text{Cu} + 2\text{Ox} \rightarrow \text{Cu}^{2+} + 2\text{Red}$ [117–120].

4.4. Local Etching of Metals and Semiconductors. Confined Etchant Layer Technique

Confined etchant layer technique [121–127] uses a SPM, in which the probe tip is replaced by a flat microTE made of Pt or Pt–Ir alloy with a pattern on the surface that should be replicated onto the substrate. Etchant E for the substrate material is not introduced into the electrolyte composition in the electrochemical cell, but is generated on the microTE as a result of oxidation of precursor P, which is present in the solution ($\text{P} \rightarrow \text{E} + n\text{e}$). The etchant diffuses to the surface of metal M substrate, which is several tens or hundreds nm apart from TE (this is the diffusion layer

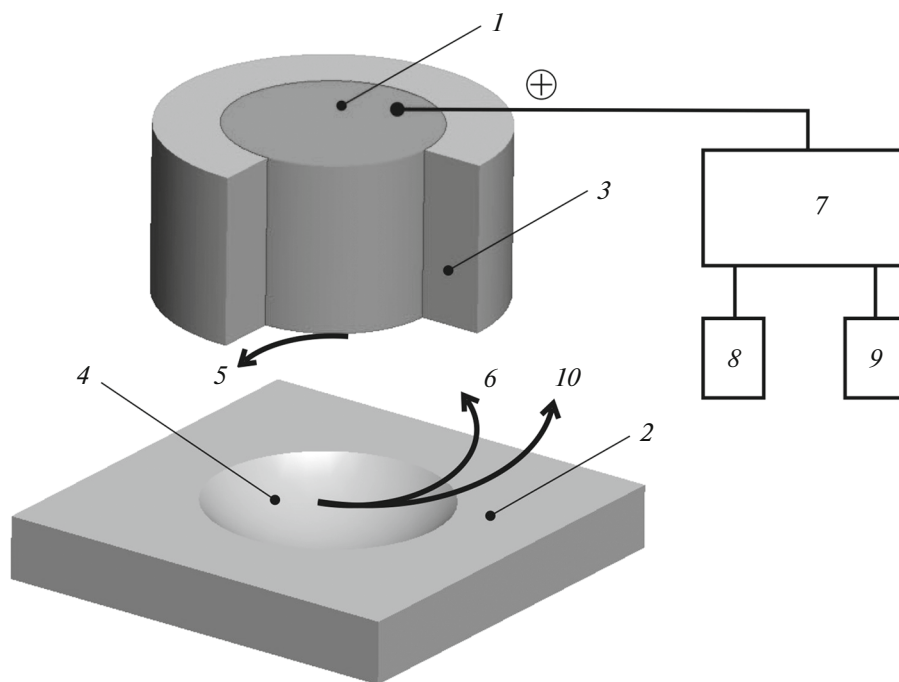


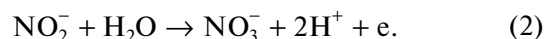
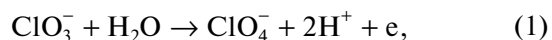
Fig. 15. Scheme of local electrochemical dissolution of metal or semiconductor substrate using SPM: (1) microelectrode (Pt), (2) substrate, (3) dielectric coating of microelectrode side surface, (4) cavity in the substrate formed by electrochemical dissolution, (5) oxidized form of redox system, (6) reduced form of redox system, (7) potentiostat, (8) reference electrode, (9) auxiliary electrode, and (10) product formed as a result of local electrochemical dissolution.

thickness near TE), and provides the etching of the required pattern with the formation of etching product R ($E + M \rightarrow P + R$). To prevent the lateral diffusion of etchant, the electrolyte contains a special substance S that plays the role of an etchant absorber ($E + S \rightarrow P + Q$, where Q is the reaction product) and thus limits the size of the etchant existence region to the space between the TE surface and the substrate surface area directly under TE. Beyond these limits, a homogeneous chemical reaction between this substance and the etchant proceeds. The higher is the metal dissolution rate, the higher is the degree of etching localization.

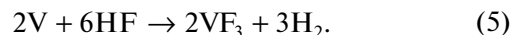
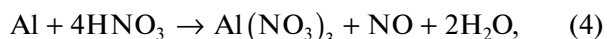
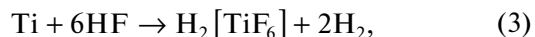
The use of microTE in the form of microwire tip easily enables ECM to be carried out at very small gaps, whereas the use of TE with a pattern for replicating it onto the substrate should have rigid size limitations to provide sufficiently intense mass transfer in a very small interelectrode space. It is necessary to provide the correct ratio between the TE surface area and the gap. Probably, etching at low current densities, for example, 5 mA/cm^2 , is largely associated with this problem [122].

In the case of local etching of titanium alloy, the solution contains the following components: 0.2 M NaF, 0.4 M NaClO_3 , 0.3 M NaNO_2 (precursors of electrochemical fabrication of etchants HF and HNO_3), 0.1 M NaOH (etchant absorber), and 0.6 M NaClO_4 . The process is performed under the galvanostatic conditions at 5 mA/cm^2 and a temperature of

$40\text{--}45^\circ\text{C}$. The following reactions proceed on the microTE [122]:



In the formed acidic environment, hydrofluoric and nitric acids play the role of etchants. Etching of titanium alloy containing Al and V proceeds by the following reactions [122]:



This technique can be used also for local etching of semiconductors.

4.5. Local Electrodeposition of Metal with Non-Electrode SPM Probe

Hirt et al. [128, 129] applied a special design of the atomic force microscope, in which the horizontal cantilever has a channel inside and ends with a short vertical nozzle. The channel is filled with the electrolyte for metal electrodeposition, in this case, copper plating sulfate electrolyte. The electrochemical cell, into which the cantilever and substrate are placed, is filled with sulfuric acid solution. The counter electrode and

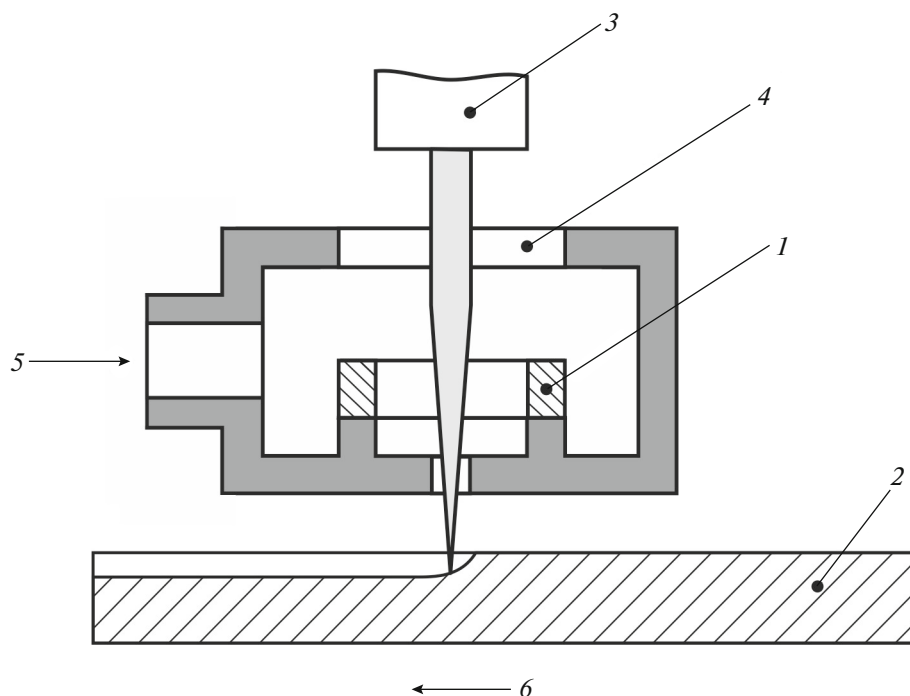


Fig. 16. Scheme of LAECM: (1) cathode, (2) workpiece, (3) laser, (4) focusing device, (5) electrolyte input, and (6) direction of workpiece motion during etching “path”.

the reference electrode are also placed into the cell. In this case, the cantilever is not an electrode. The substrate potential required for the electrodeposition is set by a potentiostat. The electrolyte for the copper deposition is supplied under a certain controlled pressure (1–25 mbar) through the cantilever to a place on the substrate where the microstructure should be formed. The localization of metal deposition is provided by the fact that the deposit forms on the substrate directly opposite the hole in the nozzle, where an electrolyte containing metal cations is supplied. At first, the authors applied this method to obtain copper islands [129] and, then, columns and more complex structures [128].

The cantilever motion according to a given program enables one to form not only vertical columns, but also various 3D structures, for example, spirals, walls of microcolumns, etc.

The authors of [128, 129] present this method as an alternative to the use of glass micropipettes.

5. LASER-ASSISTED ELECTROCHEMICAL (LAECM) AND LASER-JET ELECTROCHEMICAL MACHINING

In the LAECM method, a laser beam focused at a prescribed area on the substrate surface accelerates the electrochemical reaction many times on this area

of several units to several hundred micrometers in diameter.

For these purposes, various types of lasers, which operate in both continuous and pulsed modes, are used. The radiation power is from units of mW to several tens of watts.

This localization method is most effective under the conditions that the rate of electrochemical reaction is extremely low without the laser effect. For the anodic processes, a very low dissolution rate without laser irradiation is caused by the metal passivity. In this case, the correct electrolyte composition for machining of a particular material is important [130, 131], in particular, the presence of passivating additives ($K_2Cr_2O_7$ for etching of Al and H_3PO_4 for etching of Ti).

Figure 16 gives the simplest scheme of LAECM for local etching.

Laser stimulation of electrochemical processes is used in the case of electrode polarization with an external power source and in so-called chemical (electroless) deposition or etching of metals.

The laser radiation wavelength is chosen so as to minimize the energy absorption in the electrolyte layer through which the beam passes. The electrolyte layer for this purpose is as thin as possible, from several mm to several cm.

The main reason for a significant increase of the current density of electrochemical reaction in the region of laser action is the local heating of metal. This

follows from the results of [132–135], where it was shown that the local heating of metal by a laser or heating of bulk electrolyte leads to the same result.

Heat is generated on the irradiated electrode area as a result of absorption of laser radiation energy by the metal. The highest thermal effect is obtained at the radiation wavelength corresponding to the highest optical absorption coefficient.

The thermal properties of the substrate play an important role. On the metals with low thermal conductivity (Ni, W, Mo), the heat dissipation is lower and the degree of the process localization is higher.

The higher is the heat emission coefficient of substrate material, the faster the temperature on the irradiated area increases and reaches a certain steady-state value; however, the steady-state temperature is lower, whereas the process localization is higher [132].

In many works, laser-assisted metal deposition is performed onto the film substrates that are applied onto glass or similar materials. The results of laser-assistant deposition, the deposit thickness depend on the film thickness. This dependence was determined during the “chemical” copper deposition on the copper film of various thicknesses from the sulfate electrolyte [136]. Without the irradiation, the deposition did not occur. Under the irradiation, the deposition occurred at a film thickness larger than 12 nm and smaller than 10 μm . The latter is associated with an increase of the heat removal and a decrease of the temperature in the irradiated zone on the thicker films. The largest deposit thickness was achieved for a substrate 25 nm thick.

According to [137], the rate of local chemical deposition of nickel under the action of radiation is 20–30 times higher than in the traditional process and reached tenths of $\mu\text{m/s}$. The authors of [137] observed the natural convection near the electrode induced by the temperature gradient. The irradiation of metal substrate had an effect not only on the deposition rate, but also on the deposit structure. In this work, it was shown that the process can be intensified in the hard-to-reach places of a complex-shaped workpiece using the light supplied with fiberglass bundles.

Some disadvantage of using laser localization of chemical deposition in the electrolytes common to such processes can be a high deposition rate without laser stimulation.

The etching rate, as a rule, increases with increasing laser radiation power. When a certain power limit is exceeded, the etching rate abruptly increases due to the onset of melting of workpiece material [131, 138].

The nature of products of metal etching is of great importance. For instance, when copper is dissolved in nitric acid, the reaction products exhibit strong absorption and the application of laser for local intensification of electrochemical process is inappropriate [139].

In a number of works [140–146], the distributions of temperature and current density over the irradiated zone and adjacent areas of the substrate surface were calculated in order to determine the shape of local deposit or cavity obtained as a result of LAECM. However, this is a very complex problem to combine the heat transfer processes and the kinetics of electrochemical reactions, especially taking into account the pulsed mode of laser radiation, scanning of beam over the substrate surface, the hydrodynamic conditions, and local variation of the substrate shape with the time.

In the works on LAECM, several mechanisms of the effect of laser radiation on the electrochemical reaction rate are considered [147–149].

5.1. Effect on Equilibrium Potential

The equilibrium potential of metal in the electrolyte solution depends on the temperature. In different electrochemical systems, the dependence has different signs. Laser irradiation causes strong local heating and leads to not only a relatively high current in the irradiated zone, but also a current between the heated and cold areas of substrate surface. The current direction is determined by the sign of temperature dependence of equilibrium potential. In the case of copper in the sulfate electrolyte, copper deposition prevails on the heated area, whereas the metal etching prevails on the adjacent cold areas [150].

For nickel in the citrate electrolyte (opposite sign of the temperature dependence of potential), the opposite situation is observed: the etching on the irradiated spot and the metal deposition on the adjacent area [133].

5.2. An Increase of Reaction Rate Controlled by Charge Transfer

An increase of the current density i with increasing temperature T is described by equation $i = Ae^{-W/(RT)}$, where A is a pre-exponential factor, and W is the effective activation energy. The effect of temperature substantially depends on W .

In [135], the dependences of the laser-enhanced current for the reaction controlled by charge transfer $\delta i = \delta i_k = (i_k^{\text{las}} - i_k)/i_k$ (where i_k is the current with no laser and i_k^{las} is the laser-enhanced current) on the power w of laser radiation of various wavelength λ were determined. It was found that, first, δi_k linearly increases with increasing w , and, second, the values of δi_k at a given w and different λ values differ only slightly, except for the longwave radiation, which is considerably less efficient.

5.3. Intensification of Mass Transfer in Diffusion Boundary Layer

Under the action of laser, the temperature of solution near the substrate increases, and a gradient of density of nonuniformly heated solution arises. As a result, a laminar or, at a higher temperature, turbulent electrolyte flow arises near the electrode and intensifies mass transfer. From the theory of convective heat transfer, it is known that a laminar liquid flow, which is directed from the circle periphery to its center, arises near the heated circular surface area. In the laser-assisted electrochemical deposition of metal, the current decreases in the same direction due to a decrease of the electrolyte concentration. The deposit thickness decreases from the periphery to the center [169]; when the reaction is controlled by the charge-transfer, this does not happen. Conversely, the metal dissolution is more intense in the center of the spot and retards towards the periphery. The authors of [152] observed the formation of a crater on the galvanic deposit at a highly intense laser radiation and suggested that it was caused by vapor bubbles formed during the liquid boiling near the laser spot.

Under the turbulent conditions, intense stirring provides approximately identical mass transfer conditions over the entire heated area on the substrate surface.

The results of [135] lead to the conclusion that $\delta i_k^{\text{las}} \approx 5\delta i_d^{\text{las}}$ at a given radiation power. This reflects the fact that the activation energy of metal deposition controlled by diffusion is much lower than that controlled by charge transfer.

At a sufficient power of laser radiation, the temperature of the irradiated surface area reaches the boiling point of solution and vapor bubbles form on the electrode. The bubbles detach from the surface, stir the liquid near the electrode, and intensify the mass transfer and the reaction rate limited by the mass transfer. The local stirring combined with local heating provide a high degree of localization of electrochemical process on the irradiated electrode area.

However, stirring also leads to an increase in heat removal from the heated electrode area to the electrolyte. This will lead to a decrease of the temperature in the LAECM zone; this is especially important for the reaction controlled by charge transfer. On the other hand, blocking of the electrode with gas bubbles will lead to a decrease of heat removal from the electrode to the solution and, thus, an increase in the temperature of the electrode.

The net effect is cooling of the electrode with increasing solution stirring rate. For example, in [135, 170], it was experimentally shown that the current density of metal deposition decreases with increasing solution flow rate or the electrode rotation rate.

According to the observations of the authors of [132], an increase of the spot radius (by changing the

focusing) leads to a decrease of the temperature at the same laser radiation power. At a small spot diameter, vapor bubbles quickly form and are immediately removed from the metal electrodeposition zone. At a large spot radius, the bubbles are retained in the deposition zone, increase in size, and then detach. Therefore, it is recommended to perform the electrodeposition with strong focusing, i.e. at a high radiation power density.

5.4. Effect on Current Efficiency

When several parallel reactions proceed on the electrode, the heating caused by the laser irradiation can lead to a change in the current efficiency for the target reaction as a result of a difference between the temperature overvoltage coefficients of the target and side reactions. If the current efficiency increases with the temperature, the ratio between the process rates in the machining zone and in the adjacent area will also increase, and a degree of localization of metal electrodeposition will increase. The inverse relationship will lead to opposite effects.

A practically important example of the temperature dependence of current efficiency is the anodic dissolution of steels in the sodium nitrate solutions, when the current efficiency decreases with increasing temperature. Obviously, this is the reason for strong retardation of jet electrochemical drilling of thin holes in steel, which was observed under laser irradiation in [153]. The authors of this work consider also another possible mechanism of retardation of metal dissolution: an increase in the current efficiency of side reaction of oxygen evolution, the formation of additional current carriers in the semiconductor oxide film on the metal under the action of laser.

5.5. Effect on Metal Passivity

The depassivating effect of laser on the passive metals is very important both for the anodic dissolution and cathodic deposition and is associated primarily with heating. A sufficient increase of the temperature eliminates passivity and, thus, significantly enhances the cathodic deposition of iron group metals [154].

An increase of the temperature in the laser-irradiated zone significantly reduces the passivation limitations on the metal dissolution rate. The depassivation by laser heating to the temperatures approaching the melting points of metals enables one to replace hazardous solutions of acids and alkalis by neutral solutions of inorganic salts, for example, NaNO_3 for etching (without external power sources) of such metals as stainless steel, molybdenum, niobium, copper, and nickel [171]. In this case, some specific features may arise, in particular, the formation of salt films in the machining zone [150].

The presence or absence of passive oxide film on copper and the pH value of sulfate electrolyte during laser irradiation can determine whether the metal deposition or dissolution will occur [172].

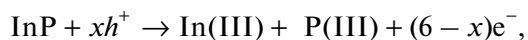
5.6. Thermal Stresses and Plastic Deformation in the Surface Metal Layer

Efimov et al. [151] studied the laser activation of nickel electrode in the 1 M H₂SO₄ solution upon the action of laser nanosecond pulses with a power of up to 50 MW/cm². The metal dissolution rate at the anodic potentials increased 10³ times. The authors indicated that the electrode activity retained for a long time after the irradiation. A significantly shorter time was required to cool the metal after a pulse. This led to the conclusion that the metal activation is non-thermal. It was supposed that the electrode processes were enhanced by the time-relaxing plastic deformation in the surface metal layer due to thermal stresses. The heated metal in the zone affected by laser radiation undergoes compressive loads from the surrounding colder metal. A nonequilibrium, higher number of dislocations exits form on the stressed surface area, which can change the overvoltage of electrochemical reaction.

5.7. LAECM of Semiconductors

The laser-assisted etching of semiconductors in the solutions is realized both due to a significant increase of the temperature in the irradiated zone and due to photogeneration of charge carriers.

The anodic dissolution of *n*-type semiconductor material is known to occur with the direct participation of minority carriers, holes, which are present in a very low concentration. Therefore, the dissolution rate is low; it is limited by a low saturation current. Laser illumination of the electrode induces intense photogeneration of holes, raises by many times the saturation current and possible etching rate of semiconductor, for example [155, 156]. For instance, in the local laser-assisted etching of *n*-InP, the photogeneration of holes involved in the etching takes place:



where *x* is the number of photons involved in the oxidation of InP molecule and (6 - *x*) is the number of not photogenerated electrons.

A number of works [156–158] are devoted to the fabrication of diffraction lattices by the method of selective interference photoetching of semiconductors.

For example, Belyakov et al. [158] obtained relief diffraction lattices with a spatial frequency above 2500 mm⁻¹. When choosing an etchant, the authors focused on the solution transparency for laser beam

and the absence of gas evolution in the etching zone. The main solutions for local etching of semiconductors are based on HF, KOH, or H₂SO₄ [138, 156–158, etc.].

Maskless laser-induced deposition of metals on semiconductor surfaces enables the formation of local deposits of 1 μm scale with a high conductivity and controlled type of contact (ohmic or barrier). It is one of the methods for fabricating various electronic devices.

The authors of [159] deposited nickel (the most suitable metal for contacts of silicon solar cells), and also copper and zinc on the substrate of *p*-type silicon single crystal with scanning a laser beam over the substrate surface. The copper deposits from a sulfate electrolyte and gold deposits from a cyanide electrolyte were obtained on GaAs [160].

Sasano et al. [161] obtained electrical contacts by the laser-assisted local potentiostatic electrodeposition of a series of copper “dots” and “patterns” on porous silicon. When a *p*-type semiconductor is placed into a solution containing metal ions, the cathodic polarization does not reduce metal ions in the dark due to a low electron content in the conduction band. Under illumination, the electrons from the valence band pass to the conduction band and can contribute to the reduction at a correct ratio between the energy levels of conduction band and the redox potential. It should be noted that the selective copper deposition by the LAECM method from the solutions of simple copper salts is hindered by immersion metal deposition not only on the illuminated areas, but on the entire specimen surface. The immersion deposition was suppressed by the introduction of chlorides into the electrolyte and complex formation with copper cations [151, 161].

The immersion deposition is typical for such noble metals as Ag, Pt, Cu, in contrast to less noble metals as Ni, Fe, Zn [162].

The complexation method can also be used for platinum or palladium deposition on silicon. These metals are catalysts for the hydrogen evolution reaction, and the deposits of these metals on silicon can be used to produce hydrogen by converting solar energy.

The work [163] showed the possibility of electroless deposition of platinum from the chloroplatinic acid solution on the *p*-type, *n*-type and undoped InP specimens under the action of pulsed laser radiation.

In a number of papers, for example [164], the works on the laser-assisted “chemical” deposition of many metals on the substrates of Si, SiC, GaAs, InP, InSe, TiO₂, etc. are cited.

Laser radiation not only promotes the deposition and dissolution of materials, but also initiates local growth of anodic oxide films on Ti, Nb, Zr, and Hf [165].

5.8. Laser-Jet Electrochemical Machining

Laser-assisted jet ECM differs from the jet ECM (section 3.5) in that a focused laser beam is directed through the nozzle for supplying electrolyte to the machining zone. Here, the electrolyte jet serves as the optical fiber.

In the indicative works, the results of jet ECM and laser-assisted jet ECM are compared.

The local gold deposition rate (the illuminated spot is 0.05 cm in diameter) on the metal substrate reaches 10–12 $\mu\text{m/s}$ [166, 167]. This is by more than an order of magnitude higher than in the jet ECM without a laser. The current efficiency of gold deposition without laser irradiation is 15–20%, whereas under the irradiation (25 W), it is about 60%. The observed shift of the polarization curve to the region of more positive potentials corresponds to a decrease of the hydrogen evolution rate.

The work [168] is devoted to cutting grooves in the specimens of aluminum, stainless steel, and titanium alloy in the NaCl or NaNO₃ solutions by these two methods. The main result is that under the action of laser radiation, the groove is deeper than without a laser (all other conditions being the same) by 10% on steel, by 20% on aluminum, and by 14% on titanium; the transverse groove size was smaller by 27% on steel, by 30% on aluminum, and by 12% on titanium. In other words, the laser effect raises the degree of localization of electrochemical process.

Datta et al. compared two methods for the dissolution of nickel and stainless steel in the NaCl and NaNO₃ solutions [153]. In ECM, the best results in terms of machining rate and accuracy were obtained in the NaNO₃ solution. Laser-assisted jet ECM in NaNO₃ appeared to be unsuitable due to a low current efficiency. Probably, this is due to a high temperature in the machining zone during LAECM (the current efficiency in this solution decreases with increasing temperature). In the case of jet LAECM, NaCl should be used; laser radiation raises a degree of dissolution localization in this electrolyte and thus significantly reduces the main disadvantage of ECM in NaCl.

6. CONCLUSIONS

The main method for localizing the deposition, dissolution, and oxidation of metals and semiconductors is the use of micro/nanoscale tool-electrodes (cathodes for dissolution and oxidation and anodes for electrodeposition) and maintaining micro/nanoscale interelectrode gaps. Additional techniques are used to increase a degree of localization, decrease the lateral distribution of electrochemical machining in the solution directly under the tool microelectrode: ultrashort voltage pulses, limited volume of electrolyte in the interelectrode space (machining through a liquid meniscus and electrochemical microcells).

An important direction in increasing a degree of localization of maskless electrochemical processes using micro/nanoscale electrodes and interelectrode gaps is the localization of electroactive component of electrolyte (ions of metal deposited on the substrate or the component responsible for the local etching of substrate) in the machining zone. This includes the use of electrolytes, which are free of electroactive component in their bulk. The electroactive component forms on the tool-electrode or is introduced into the electrochemical cell directly to the substrate zone intended for machining. A special component, the absorbent of electroactive component that limits its lateral diffusion, included into the electrolyte composition enables one to increase the degree of localization.

A specific area is the localization by focused laser radiation.

The limited size of review allowed us to touch on not all aspects of the problem and quote only a relatively small number of published works on this rapidly developing field of application of electrochemical methods in the interdisciplinary interests. The reader can find many references to other works in the publications cited here.

FUNDING

The work was performed with support of Ministry of Science and Higher Education of Russian Federation.

CONFLICT OF INTEREST

The authors declare that they have no conflicts of interest.

REFERENCES

1. *Electrochemical Microsystem Technologies*, Schultze, J.W., Osaka, T., and Datta, M., Eds., London: Taylor & Francis, 2002.
2. Datta, M. and Landolt, D., Fundamental aspects and applications of electrochemical microfabrication, *Electrochim. Acta*, 2000, vol. 45, p. 2535.
3. Bhattacharyya, B., *Electrochemical Micromachining for Nanofabrication, MEMS and Nanotechnology*, Oxford: William Andrew, 2015.
4. Braun, T.M. and Schwartz, D.T., The emerging role of electrodeposition in additive manufacturing, *Electrochem. Soc. Interface*, 2016, vol. 25, no. 1, p. 69.
5. Liu, Y., Zeng, Y., and Yu, H., Development of micro-electrodes for electrochemical machining, *Int. J. Manuf. Technol.*, 2011, vol. 55, p. 195.
6. Kim, B.H., Na, C.W., Lee, Y.S., Choi, D.K., and Chu, C.N., *Micro electrochemical machining of 3D micro structure using dilute sulfuric acid*, *CIRP Annals – Manufacturing Technology*, 2005, vol. 54, p. 191.
7. Wang, Y., Zeng, Y., Qu, N., and Zhu, D., Electrochemical micromachining of small tapered microstructures with sub-micro spherical tool, *Int. J. Adv. Manuf. Technol.*, 2016, vol. 84, p. 851.

8. Koch, M., Kirchner, V., and Schuster, R., Electrochemical micromachining with ultrashort voltage pulses, *Electrochim. Acta*, 2003, vol. 48, p. 3213.
9. Sjöström, T. and Su, B., Micropatterning of titanium surfaces using electrochemical micromachining with an ethylene glycol electrolyte, *Mater. Lett.*, 2011, vol. 65, p. 3489.
10. Maurer, J.J., Mallett, J.J., Hudson, J.L., Fick, S.E., Moffat, T.P., and Shaw, G.A., Electrochemical micromachining of Hastelloy B-2 with ultrashort voltage pulses, *Electrochim. Acta*, 2010, vol. 55, p. 952.
11. Park, B.J., Kim, B.H., and Chu, C.N., The effects of tool electrode size on characteristics of micro electrochemical machining, *Annals of the CIRP*, 2006, vol. 55, p. 197.
12. Koza, J.A., Sueptitz, R.S., Uhlemann, M., Schutz, L., and Gebert, A., Electrochemical micromachining of a Zr-based bulk metallic glass using a micro-tool electrode technique, *Intermetallics*, 2011, vol. 19, p. 437.
13. Li, Y., Ma, X., Liu, G., Hu, M., and Yi, F., Research on micro ECM using micro array electrode, *Proc. 16th Int. Symp. on Electromachining*, Shanghai, China, 2010, p. 335.
14. Sedykin, F.V., *Razmernaya elektrokhimicheskaya obrabotka detalei mashin* (Electrochemical Machining of Machine Parts), Moscow: Mashinostroenie, 1976.
15. Rumyantsev, E. and Davydov, A., *Electrochemical Machining of Metals*, Moscow: Mir, 1989.
16. Davydov, A.D., Volgin, V.M., and Lubimov, V.V., Electrochemical machining of metals: fundamentals of electrochemical shaping, *Russian J. Electrochem.*, 2004, vol. 40, p. 1230.
17. Wang, Z., Zhu, Y., Fan, Z., and Yun, N., Mechanism and process study of ultrasonical vibration combined synchronizing pulse electrochemical micro-machining, *Proc. 16th Int. Symp. on Electromachining*, Shanghai, China, 2010, p. 351.
18. Zhitnikov, V.P. and Zaitsev, A.N., *Impul'snaya elektrokhimicheskaya razmernaya obrabotka* (Pulsed Electrochemical Machining), Moscow: Mashinostroenie, 2008.
19. Schramm, A., *Gesetzmäßigkeiten des elektrochemischen abtrags beim kombinierten elektrochemischen/ultraschall-senken*, *Fertigungstech. Betr.*, 1985, vol. 35, p. 367.
20. Allongue, P., Jiang, P., Kirchner, V., Trimmer, A.L., and Schuster, R., Electrochemical micromachining of p-type silicon, *J. Phys. Chem. B.*, 2004, vol. 108, p. 14434.
21. Trimmer, A.L., Maurer, J.J., Schuster, R., Zangari, G., and Hudson, J.L., All-electrochemical synthesis of submicrometer Cu structures on electrochemically machined p-Si substrates, *Chem. Mater.*, 2005, vol. 17, p. 6755.
22. Schuster, R., Kirchner, V., Allongue, P., and Ertl, G., Electrochemical micromachining, *Science*, 2000, vol. 289, p. 98.
23. Koch, M., Kirchner, V., and Schuster, R., Electrochemical micromachining with ultrashort voltage pulses, *Electrochim. Acta*, 2003, vol. 48, p. 3213.
24. Kirchner, V., Xia, X., and Schuster, R., Electrochemical nanostructuring with ultrashort voltage pulses, *Acc. Chem. Res.*, 2001, vol. 34, p. 371.
25. Park, B.J., Kim, B.H., and Chu, C.N., The effects of tool electrode size on characteristics of micro electrochemical machining, *Annals of the CIRP*, 2006, vol. 55, p. 197.
26. Madden, J.D., Lafontaine, S.R., and Hunter, I.W., Fabrication by electrodeposition: building 3D structures and polymer actuators, *Proc. Sixth Int. Symp. "Micro Machine and Human Science"*, Nagoya, Japan, 1995, p. 77.
27. Madden, J.D. and Hunter, I.W., Three-dimensional microfabrication by localized electrochemical deposition, *J. Microelectromech. Syst.*, 1996, vol. 5, no. 1, p. 24.
28. Said, R.A., Microfabrication by localized electrochemical deposition: experimental investigation and theoretical modeling, *Nanotechnology*, 2003, vol. 14, no. 5, p. 523.
29. Lin, J.C., Jang, S.B., Lee, D.L., Chen, C.C., Yeh, P.C., Chang, T.K., and Yang, J.H., Fabrication of micrometer Ni columns by continuous and intermittent microanode guided electroplating, *J. Micro-mech. Microeng.*, 2005, vol. 15, no. 12, p. 2405.
30. Lin, C.S., Lee, C.Y., Yang, J.H., and Huang, Y.S., Improved copper microcolumn fabricated by localized electrochemical deposition, *Electrochem. Solid-State Lett.*, 2005, vol. 8, p. C125.
31. Seol, S.-K., Pyun, A.-R., Hwu, Y., Margaritondo, G., and Je, J.-H., Localized electrochemical deposition of copper monitored using real-time x-ray microradiography, *Adv. Funct. Mater.*, 2005, vol. 15, p. 934.
32. Yang, J.H., Lin, J.C., Chang, T.K., You, X.B., and Jiang, S.B., Localized Ni deposition improved by saccharin sodium in the intermittent MAGE process, *J. Micromech. Microeng.*, 2009, vol. 19, p. 025015.
33. Yang, J.H., Lin, J.C., Chang, T.K., Lai, G.Y., and Jiang, S.B., Assessing the degree of localization in localized electrochemical deposition of copper, *J. Micromech. Microeng.*, 2008, vol. 18, p. 055023.
34. Lin, J.C., Yang, J.H., Chang, T.K., and Jiang, S.B., On the structure of micrometer copper features fabricated by intermittent micro-anode guided electroplating, *Electrochim. Acta*, 2009, vol. 54, no. 24, p. 5703.
35. Lin, J.C., Chang, T.K., Yang, J.H., Chen, Y.S., and Chuang, C.L., Localized electrochemical deposition of micrometer copper columns by pulse plating, *Electrochim. Acta*, 2010, vol. 55, p. 1888.
36. Said, R.A., Localized electro-deposition (LED): the march toward process development, *Nanotechnology*, 2004, vol. 15, p. S649.
37. Lin, J.C., Chang, T.K., Yang, J.H., Jeng, J.H., Lee, D.L., and Jiang, S.B., Fabrication of a micrometer Ni-Cu alloy column coupled with a Cu micro-column for thermal measurement, *J. Micromech. Microeng.*, 2009, vol. 19, p. 015030(1-10).
38. Debnath, S., Laskar, H.R., and Bhattacharyya, B., Investigation into generation of micro features by localized electrochemical deposition, *J. Inst. Eng. India Ser. C*, 2019, vol. 100, no. 1, p. 113.

39. Wang, F., Xiao, H., and He, H., Effects of applied potential and the initial gap between electrodes on localized electrochemical deposition of micrometer copper columns, *PMC, Scientific Reports*, 2016, no. 6, p. 26270. <https://doi.org/10.1038/srep26270>
40. Lee, C.-Y., Lin, C.-S., and Lin, B.-R., Localized electrochemical deposition process improvement by using different anodes and deposition directions, *J. Micromech. Microeng.*, 2008, vol. 18, p. 105008.
41. El-Giar, E.M., U, C., and Thomson, D.J., Localized electrochemical plating of interconnectors for microelectronics, *Proc. 1997 Conf. on Communications, Power and Computing WESCANEX'97*, Winnipeg, MB, 1997, p. 327.
42. Jansson, A., Thornell, G., and Johansson, S., High resolution 3D microstructures made by localized electrodeposition of nickel, *J. Electrochem. Soc.*, 2000, vol. 147, no. 5, p. 1810.
43. Hwang, Y.-R., Lin, J.-C., and Chen, T.-C., The analysis of the deposition rate for continuous micro-anode guided electroplating process, *Int. J. Electrochem. Sci.*, 2012, vol. 7, p. 1359.
44. Pellicer, E., Pané, S., Panagiotopoulou, V., Fusco, S., Sivaraman, K.M., Suriñach, S., Baró, M.D., Nelson, B.J., and Sort, J., Localized electrochemical deposition of porous Cu–Ni microcolumns: Insights into the growth mechanisms and the mechanical performance, *Int. J. Electrochem. Sci.*, 2012, vol. 7, p. 4014.
45. Chang, T.K., Lin, J.C., Yang, J.H., Yeh, P.C., Lee, D.L., and Jiang, S.B., Surface and transverse morphology of micrometer nickel columns fabricated by localized electrochemical deposition, *J. Micromech. Microeng.*, 2007, vol. 17, p. 2336.
46. Yeo, S.H. and Choo, J.H., Effects of rotor electrode in the fabrication of high aspect ratio microstructures by localized electrochemical deposition, *J. Micromech. Microeng.*, 2001, vol. 11, p. 435.
47. Wang, F., Bian, H., Wang, F., Sun, J., and Zhu, W., Fabrication of micro copper walls by localized electrochemical deposition through the layer by layer movement of a micro anode, *J. Electrochem. Soc.*, 2017, vol. 164, p. D758.
48. Wang, F., Sun, J., Liu, D., Wang, Y., and Zhu, W., Effect of voltage and gap on micro-nickel-column growth patterns in localized electrochemical deposition, *J. Electrochem. Soc.*, 2017, vol. 164, p. D297.
49. Yeo, S.H., Choo, J.H., and Sim, K.H.A., On the effects of ultrasonic vibrations on localized electrochemical deposition, *J. Micromech. Microeng.*, 2002, vol. 12, p. 271.
50. Said, R.A., Alshwawreh, N., and Haik, Y., Fabrication of array microstructures using serial and parallel localized electrodeposition, *Int. J. Nanosci.*, 2009, vol. 8, no. 03, p. 323.
51. Ciou, Y.J., Hwang, Y.R., and Lin, J.C., Theoretical modeling and fabrication of two-dimensional microstructures by using micro-anode-guided electroplating with real-time image processing, *Key Eng. Mat.*, 2015, vol. 656, p. 604.
52. Brant, A.M., Sundaram, M.M., and Kamaraj, A.B., Finite element simulation of localized electrochemical deposition for maskless electrochemical additive manufacturing, *J. Manuf. Sci. E.-T. ASME*, 2015, vol. 137, no. 1, p. 011018.
53. Xiao, H., Zeng, P., Ren, X., and Wang, F., Three-dimensional microfabrication of copper column by localized electrochemical deposition, *Electronic Packaging Technology (ICEPT), 17th Int. Conference IEEE*, 2016, p. 69.
54. Kamaraj, A., Lewis, S., and Sundaram, M., Numerical study of localized electrochemical deposition for micro electrochemical additive manufacturing, *Procedia CIRP*, 2016, vol. 42, p. 788.
55. Volgin, V.M., Kabanova, T.B., and Davydov, A.D., Modeling of local maskless electrochemical deposition of metal microcolumns, *Chem. Eng. Sci.*, 2018, vol. 183, p. 123.
56. Ullmann, R., Will, T., and Kolb, D.M., Nanoscale decoration of Au(111) electrodes with Cu clusters by an STM, *Chem. Phys. Lett.*, 1993, vol. 209, p. 238.
57. Ullmann, R., Will, T., and Kolb, D.M., Nanostructuring of electrode surfaces by tip-induced metal deposition, *Ber. Bunsenges. Phys. Chem.*, 1995, vol. 99, p. 1414.
58. Engelmann, G.E., Ziegler, J.C., and Kolb, D.M., Electrochemical fabrication of large arrays of metal nanoclusters, *Surf. Sci. Lett.*, 1998, vol. 401, p. L420.
59. Kolb, D.M., Ullmann, R., and Will, T., Nanofabrication of small copper clusters on gold (111) electrodes by a scanning tunneling microscope, *Science*, 1997, vol. 275, p. 1097.
60. Kolb, D.M., Ullmann, R., and Ziegler, J.C., Electrochemical nanostructuring, *Electrochim. Acta*, 1998, vol. 43, p. 2751.
61. Engelmann, G.E., Ziegler, J.C., and Kolb, D.M., Nanofabrication of small palladium clusters on Au(111) electrodes with a scanning tunneling microscope, *J. Electrochem. Soc.*, 1998, vol. 145, p. L33.
62. Hofmann, D., Schindler, W., and Kirschner J., Electrodeposition of nanoscale magnetic structures, *Appl. Phys. Lett.*, 1998, vol. 73, p. 3279.
63. Schindler, W., Hofmann, D., and Kirschner, J., Nanoscale electrodeposition: A new route to magnetic nanostructures? *J. Appl. Phys.*, 2000, vol. 87, p. 7007.
64. Schindler, W., Hofmann, D., and Kirschner J., Localized electrodeposition using a scanning tunneling microscope tip as a nanoelectrode, *J. Electrochem. Soc.*, 2001, vol. 148, p. C124.
65. Spiegel, A., Staemmler, L., Döbeli, M., and Schmuki, P., Selective electrodeposition of Cu nanostructures on focused ion beam sensitized p-Si, *J. Electrochem. Soc.*, 2002, vol. 149, p. C432.
66. Homma, T., Kubo, N., and Osaka, T., Maskless and electroless fabrication of patterned metal nanostructures on silicon wafers by controlling local surface activities, *Electrochim. Acta*, 2003, vol. 48, p. 3115.
67. Choi, J., Chen, Z., and Singh, R.K., A method for selective deposition of copper nanoparticles on silicon surfaces, *J. Electrochem. Soc.*, 2003, vol. 150, p. C563.

68. Schmuki, P. and Erickson, L.E., Selective high-resolution electrodeposition on semiconductor defect patterns, *Phys. Rev. Lett.*, 2000, vol. 85, p. 2985.
69. Santinacci, L., Djenizian, T., and Schmuki, P., Atomic force microscopy-induced nanopatterning of Si(100) surfaces, *J. Electrochem. Soc.*, 2001, vol. 148, p. C640.
70. Pötzschke, R.T., Staikov, G., Lorenz, W.J., and Wiesbeck, W., Electrochemical nanostructuring of *n*-Si(111) single-crystal faces, *J. Electrochem. Soc.*, 1999, vol. 146, p. 141.
71. Ammann, E. and Mandler, D., Local deposition of gold on silicon by the scanning electrochemical microscope, *J. Electrochem. Soc.*, 2001, vol. 148, p. 533.
72. Oskam, G., Long, J.G., Natarajan, A., and Searson, P.C., Electrochemical deposition of metals onto silicon, *J. Phys. D: Appl. Phys.*, 1998, vol. 31, p. 1927.
73. Avouris, P., Hertel, T., and Martel, R., Atomic force microscope tip-induced local oxidation of silicon: kinetics, mechanism, and nanofabrication, *Appl. Phys. Lett.*, 1997, vol. 71, p. 285.
74. Avouris, P., Martel, R., Hertel, T., and Sandstrom, R.L., AFM-tip-induced and current-induced local oxidation of silicon and metals, *Appl. Phys. A: Mater. Sci. Process.*, 1998, vol. 66, p. S659.
75. Held, R., Heinzl, T., Studerus, P., and Ensslin, K., Nanolithography by local anodic oxidation of metal films using an atomic force microscope, *Physica E: Low-Dimensional Systems and Nanostructures*, 1998, vol. 2, p. 748.
76. Vaccaro, P.O., Sakata, S., Yamaoka, S., Umez, I., and Sugimura, A., Nano-oxidation of vanadium thin films using atomic force microscopy, *J. Mater. Sci. Lett.*, 1998, vol. 17, p. 1941.
77. Okur, S., Büyükköse, S., and Tari, S., Scanning probe oxidation lithography on Ta thin films, *J. Nanosci. Nanotechnol.*, 2008, vol. 8, p. 5640.
78. Matsumoto, K., Takahashi, S., Ishii, M., Hoshi, M., Kurokawa, A., Ichimura, S., and Ando, A., Application of STM nanometer-size oxidation process to planar-type MIM diode, *Jpn. J. Appl. Phys.*, 1995, vol. 34, p. 1387.
79. Snow, E.S. and Campbell, P.M., Fabrication of Si nanostructures with an atomic force microscope, *Appl. Phys. Lett.*, 1994, vol. 64, p. 1932.
80. Sugimura, H., Uchida, T., Kitamura, N., and Masuhara, H., Tip-induced anodization of titanium surfaces by scanning tunneling microscopy: a humidity effect on nanolithography, *Appl. Phys. Lett.*, 1993, vol. 63, p. 1288.
81. Snow, E.S., Park, D., and Campbell, P.M., Single-atom point contact devices fabricated with an atomic force microscope, *Appl. Phys. Lett.*, 1996, vol. 69, p. 269.
82. Campbell, P.M., Snow, E.S., and McMarr, P.J., Fabrication of nanometer-scale side-gated silicon field effect transistors with an atomic force microscope, *Appl. Phys. Lett.*, 1995, vol. 66, p. 1388.
83. Day, H.C. and Allee, D.R., Selective area oxidation of silicon with a scanning force microscope, *Appl. Phys. Lett.*, 1993, vol. 62, p. 2691.
84. Vullers, R.J.M., Ahlskog, M., and Van Haesendonck, C., Titanium nanostructures made by local oxidation with the atomic force microscope, *Appl. Surface Sci.*, 1999, vol. 144, p. 584.
85. Sugimura, H., Uchida, T., Kitamura, N., and Masuhara, H., Scanning tunneling microscope tip-induced anodization for nanofabrication of titanium, *J. Phys. Chem.*, 1994, vol. 98, p. 4352.
86. Wang, D., Tsau, L., Wang, K.L., and Chow, P., Nanofabrication of thin chromium film deposited on Si(100) surfaces by tip induced anodization in atomic force microscopy, *Appl. Phys. Lett.*, 1995, vol. 67, p. 1295.
87. Seol, S.K., Kim, D., Lee, S., Kim, J.H., Chang, W.S., and Kim, J.T., Electrodeposition-based 3D printing of metallic microarchitectures with controlled internal structures, *Small*, 2015, vol. 11, p. 3896.
88. Morsali, S., Daryadel, S., Zhou, Z., Behroozfar, A., Baniyadi, M., Qian, D., and Minary-Jolandan, M., Multi-physics simulation of metal printing at micro/nanoscale using meniscus-confined electrodeposition: Effect of environmental humidity, *J. Appl. Phys.*, 2017, vol. 121, p. 024903.
89. Suryavanshi, A.P. and Yu, M.-F., Electrochemical fountain pen nanofabrication of vertically grown platinum nanowires, *Nanotechnology*, 2007, vol. 18, p. 105305.
90. Morsali, S., Daryadel, S., Zhou, Z., Behroozfar, A., Baniyadi M., Moreno, S., Qian, D., and Minary-Jolandan, M., Multi-physics simulation of metal printing at micro/nanoscale using meniscus-confined electrodeposition: Effect of nozzle speed and diameter, *J. Appl. Phys.*, 2017, vol. 121, p. 214305.
91. Suryavanshi, A.P. and Yu, M.-F., Probe-based electrochemical fabrication of freestanding Cu nanowire array, *Appl. Phys. Lett.*, 2006, vol. 88, p. 083103.
92. Hu, J. and Yu, M.-F., Meniscus-confined three-dimensional electrodeposition for direct writing of wire bonds, *Science*, 2010, vol. 329, p. 313.
93. Chen, X., Liu, X., Childs, P., Brandon, N., and Wu, B., A low cost desktop electrochemical metal 3D printer, *Adv. Mater. Technol.*, 2017, vol. 2, p. 1700148.
94. Momotenko, D., Page, A., Adobes-Vidal, M., and Unwin, P.R., Write-read 3D patterning with a dual-channel nanopipette, *ACS Nano*, 2016, vol. 10, p. 8871.
95. Müller, A.D., Müller, F., and Hietschold, M., Electrochemical pattern formation in a scanning near-field optical microscope, *Appl. Phys. A: Mater. Sci. Process.*, 1998, vol. 66, p. S453.
96. Ito, S. and Iwata, F., Nanometer-scale deposition of metal plating using a nanopipette probe in liquid condition, *Jpn. J. Appl. Phys.*, 2011, vol. 50, p. 08LB15.
97. Leichlé, T. and Nicu, L., Copper electrodeposition localized in picoliter droplets using microcantilever arrays, *Appl. Phys. Lett.*, 2006, vol. 88, p. 254108.
98. Pirani, M. and Schöter, K., Elektrolytische formgebung von harten metallischen gegenständen, *Z. Metallkunde*, 1924, vol. 16, p. 132.
99. Lohregel, M.M., Klüppel, I., Rosenkranz, C., Betermann, H., and Schultze, J.W., Microscopic investi-

- gations of electrochemical machining of Fe in NaNO_3 , *Electrochim. Acta*, 2003, vol. 48, p. 3203.
100. Cowper-Coles, S., An electrolytic drilling and slotting process, *The Electro-Chemist and Metallurgist*, 1903, vol. 3, part 4, p. 203.
101. Cowper-Coles, S., Electrolytic drilling and slotting process, *Electrochemical Industry*, 1904, vol. 2, no. 1, p. 28.
102. Nelson, J.B., Wisecarver, Z., and Schwartz, D.T., Electrochemical printing: mass transfer effects, *J. Micromech. Microeng.*, 2007, vol. 17, p. 1192.
103. Cole, R.R. and Hopenfeld, Y., An investigation of electrolytic jet polishing at high current densities, *J. Eng. Ind., Trans. ASME*, 1963, vol. 85, no. 4, p. 395.
104. Speidel, A., Mitchell-Smith, J., Bisterov, I., and Clare, A.T., The dependence of surface finish on material precondition in electrochemical jet machining, *Proc. CIRP*, 2018, vol. 68, p. 477.
105. Li, Q. and Walker, J.D.A., Prediction of electrodeposition rates from an impinging jet, *AIChE J.*, 1996, vol. 42, p. 391.
106. Mitchell-Smith, J., Speidel, A., and Clare, A.T., Advancing electrochemical jet methods through manipulation of the angle of address, *J. Mater. Process. Technol.*, 2018, vol. 255, p. 364.
107. Natsu, W., Ikeda, T., and Kunieda, M., Generating complicated surface with electrolyte jet machining, *Precis. Eng.*, 2007, vol. 31, p. 33.
108. Natsu, W., Ooshiro, S., and Kunieda, M., Research on generation of three-dimensional surface with micro-electrolyte jet machining, *CIRP J. Manufact. Sci. Technol.*, 2008, vol. 1, p. 27.
109. Kuhn, D., Martin, A., Eckart, C., Sieber, M., Morgenstern, R., Hackert-Oschätzchen, M., Lampke, T., and Schubert, A., Localised anodic oxidation of aluminium material using a continuous electrolyte jet, *IOP Conf. Ser.: Mater. Sci. Eng.*, 2017, vol. 181, p. 012042.
<https://doi.org/10.1088/1757-899X/181/1/012042>
110. Aerts, T., De Graeve, I., Nelissen, G., Deconinck, J., Kubacki, S., Dick, E., and Terryn, H. Experimental study and modelling of aluminium in a wall-jet electrode set-up in laminar and turbulent regime, *Corros. Sci.*, 2009, vol. 51, p. 1482.
111. Meltzer, S. and Mandler, D., Microwriting of gold patterns with the scanning electrochemical microscope, *J. Electrochem. Soc.*, 1995, vol. 142, p. L82.
112. De Abril, O., Mandler, D., and Unwin, P.R., Local cobalt electrodeposition using the scanning electrochemical microscope, *Electrochem. Solid-State Lett.*, 2004, vol. 7, p. C71.
113. Borgwarth, K. and Heinze, J., Increasing the resolution of the scanning electrochemical microscope using a chemical lens: Application to silver deposition, *J. Electrochem. Soc.*, 1999, vol. 146, p. 3285.
114. Borgwarth, K., Ricken, C., Ebling, D.G., and Heinze, J., Surface characterisation and modification by the scanning electrochemical microscope (SECM), *Ber. Bunsenges. Phys. Chem.*, 1995, vol. 99, p. 1421.
115. Mandler, D. and Bard, A., High resolution etching of semiconductors by the feedback mode of the scanning electrochemical microscope, *J. Electrochem. Soc.*, 1990, vol. 137, p. 2468.
116. Sheffer, M. and Mandler, D., Scanning electrochemical imprinting microscopy: A tool for surface patterning, *J. Electrochem. Soc.*, 2008, vol. 155, p. D203.
117. Mandler, D. and Bard, A., Scanning electrochemical microscopy: The application of the feedback mode for high resolution copper etching, *J. Electrochem. Soc.*, 1989, vol. 136, p. 3143.
118. Sheffer, M. and Mandler, D., Why is copper locally etched by scanning electrochemical microscopy? *J. Electroanal. Chem.*, 2008, vol. 622, p. 115.
119. Macpherson, J.V., Slevin, C.J., and Unwin, P.R., Probing the oxidative etching kinetics of metals with the feedback mode of the scanning electrochemical microscope, *J. Chem. Soc., Faraday Trans.*, 1996, vol. 92, p. 3799.
120. Cornut, R., Nunige, S., Lefrou, C., and Kanoufi, F., Local etching of copper films by the scanning electrochemical microscope in the feedback mode: A theoretical and experimental investigation, *Electrochim. Acta*, 2011, vol. 56, p. 10701.
121. Tian, Z., Fen, Z., Tian, Z., Zhuo, X., Mu, J., Li, C., Lin, H., Ren, B., Xie, Z., and Hu, W., Confined etchant layer technique for two-dimensional lithography at high resolution using electrochemical scanning tunneling microscopy, *Faraday Discuss.*, 1992, vol. 94, p. 37.
122. Jiang, L.M., Li, W., Attia, A., Cheng, Z.Y., Tang, J., Tian, Z.Q., and Tian, Z.W., A potential method for electrochemical micromachining of titanium alloy $\text{Ti}_6\text{Al}_4\text{V}$, *J. Appl. Electrochem.*, 2008, vol. 38, p. 785.
123. Jiang, L.M., Liu, Z.F., Tang, J., Zhang, L., Shi, K., Tian, Z.Q., Liu, P.K., Sun, L.N., and Tian, Z.W., Three-dimensional micro-fabrication on copper and nickel, *J. Electroanal. Chem.*, 2005, vol. 581, p. 153.
124. Ma, X.-Z., Zhang, L., Cao, G.-H., Lin, Y., and Tang, J., Electrochemical micromachining of nitinol by confined-etchant-layer technique, *Electrochim. Acta*, 2007, vol. 52, p. 4191.
125. Zu, Y., Xie, L., Mao, B., and Tian, Z., Studies on silicon etching using the confined etchant layer technique, *Electrochim. Acta*, 1998, vol. 43, p. 1683.
126. Sun, J.J., Huang, H.G., Tian, Z.Q., Xie, L., Luo, J., Ye, X.Y., Zhou, Z.Y., Xia, S.H., and Tian, Z.W., Three-dimensional micromachining for microsystems by confined etchant layer technique, *Electrochim. Acta*, 2001, vol. 47, p. 95.
127. Yuan, Y., Han, L., Zhang, J., Jia, L., Zhao, X., Cao, Y., Hu, Z., Yan, Y., Dong, S., Tian, Z.-Q., Tian, Z.-W., and Zhan, D., Electrochemical mechanical micromachining based on confined etchant layer technique, *Faraday Discuss.*, 2013, vol. 164, p. 189.
128. Hirt, L., Ihle, S., Pan, Z., Dorwling-Carter, L., Reiser, A., Wheeler, J.M., Prolenak, R., Vörös, J., and Zambelli, T., Template-free 3D microprinting of metals using a force-controlled nanopipette for layer-by-layer electrodeposition, *Adv. Mater.*, 2016, vol. 28, p. 2311.
129. Hirt, L., Grüter, R.R., Berthelot, T., Cornut, R., Vörös, J., and Zambelli, T., Local surface modifica-

- tion via confined electrochemical deposition with FluidFM, *RSC Adv.*, 2015, vol. 5, p. 84517.
130. Tsao, J.Y. and Ehrlich, D.J., Laser-controlled chemical etching of aluminum, *Appl. Phys. Lett.*, 1983, vol. 43, p. 146.
 131. Nowak, R. and Metev, S., Thermochemical laser etching of stainless steel and titanium in liquids, *Phys.*, 1996, vol. A 63, p. 133.
 132. Hsiao, M.C. and Wan, C.C., The investigations of laser-enhanced copper plating on a good heat conducting copper foil, *J. Electrochem. Soc.*, 1991, vol. 138, p. 2273.
 133. Puippe, J.C., Acosta, R.E., and von Gutfeld, R.J., Investigation of laser-enhanced electroplating mechanisms, *J. Electrochem. Soc.*, 1981, vol. 128, p. 2539.
 134. Von Gutfeld, R.J., Tynan, E.E., Melcher, R.L., and Blum, S.E., Laser enhanced electroplating and maskless pattern generation, *Appl. Phys. Lett.*, 1979, vol. 35, p. 651.
 135. Bindra, P., Arbach, G.V., and Stimming, U., On the mechanism of laser enhanced plating of copper, *J. Electrochem. Soc.*, 1987, vol. 134, p. 2893.
 136. Al-Sufi, A.K., Eichler, H.J., and Salk, J., Laser induced copper plating, *J. Appl. Phys.*, 1983, vol. 54, p. 3629.
 137. Eremenko, A.A., Kozlova E.K., Portnyagin A.I., Romanchenko, A.N., and Filippov, A.E., Influence of optical radiation on electroless nickel plating, *Soviet J. Quantum Electronics*, 1984, vol. 14, no. 8, p. 1129.
 138. Von Gutfeld, R.J. and Hodgson, R.T., Laser enhanced etching in KOH, *Appl. Phys. Lett.*, 1982, vol. 40, p. 352.
 139. Seryanov, Yu.V., Rabkin, V.B., and Surmenko, L.A., Laser-enhanced copper etching in nitric acid solutions, *Soviet Electrochem.*, 1988, vol. 24, p. 842.
 140. Dikumar, A.I., Engelgardt, G.P., and Molin, A.N., *Termokineticheskie yavleniya pri vysokoskorostnykh elektrodnykh protsessakh* (Thermokinetic Phenomena at High-Rate Electrode Processes), Kishinev: Shtiintsa, 1989, p. 112.
 141. Yung, E.K., Hussey, B.W., Gupta, A., and Romankiw, L.T., Laser-assisted etching of manganese-zinc-ferrite, *J. Electrochem. Soc.*, 1989, vol. 136, p. 665.
 142. Seryanov, Yu.V., Grigor'eva, E.M., Bol'shinskova, T.A., and Fomenko, L.A., Thermal conditions and kinetics of formation of nickel "lines" during laser radiation of $Ni_mL_nX_k$ films on Al_2O_3 , *Fiz. Khim. Obrab. Mater.*, 1995, no. 1, p. 17.
 143. Zhang, H. and Xu, J., Modeling and experimental investigation of laser drilling with jet electrochemical machining, *Chinese J. Aeronautics*, 2010, vol. 23, p. 454.
 144. Kuiken, H.K., Mikkers, F.E.P., and Wierenga, P.E., Laser-enhanced electroplating on good heat-conducting bulk materials, *J. Electrochem. Soc.*, 1983, vol. 130, p. 554.
 145. Hsiao, M.C. and Wan, C.C., The effect of pH on the localized etching process induced by laser irradiation, *J. Electrochem. Soc.*, 1994, vol. 141, p. 943.
 146. Dzhunushaliev, V.D. and Chokoev, E.S., Specific features of laser treatment of metal in liquid, *Fiz. Khim. Obrab. Mater.*, 1990, no. 4, p. 140.
 147. Davydov, A.D., Laser electrochemical machining of metals, *Russian J. Electrochem.*, 1994, vol. 30, p. 871.
 148. Kozak, J. and Rajurkar, K.P., *Laser assisted electrochemical machining*, *Trans. NAMRI/SME*, 2001, vol. 29, p. 421.
 149. Metev, S.M. and Veiko, V.P., *Laser-Assisted Microtechnology*, Berlin: Springer, 1998.
 150. Von Gutfeld, R.J., Vigliotti, D.R., and Datta, M., Laser chemical etching of metals in sodium nitrate solution, *J. Appl. Phys.*, 1988, vol. 64, p. 5197.
 151. Efimov, I.O., Krivenko, A.G., and Benderskii, V.A., Laser activation of nickel electrodes, *Soviet Electrochemistry*, 1988, vol. 24, p. 1092.
 152. Jacobs, J.W.M. and Rikken, J.M.G., Boiling effects and bubble formation at the solid-liquid interface during laser-induced metal deposition, *J. Electrochem. Soc.*, 1987, vol. 134, p. 2690.
 153. Datta, M., Romankiw, L.T., Vigliotti, D.R., and von Gutfeld R.J., Jet and laser-jet electrochemical micro-machining of nickel and steel, *J. Electrochem. Soc.*, 1989, vol. 136, p. 2251.
 154. Vagramyan, A.T. and Zhamagortsyants, M.A., *Elektroosazhdenie metallov i ingibiruyushchaya adsorbtsiya* (Electrodeposition of Metals and Inhibiting Adsorption), Moscow: Nauka, 1969, p. 91.
 155. Shor, J.S., Zhang, X.G., and Osgood, R.M., Laser-assisted photoelectrochemical etching of *n*-type beta-SiC, *J. Electrochem. Soc.*, 1992, vol. 139, p. 1213.
 156. Lum, R.M., Glass, A.M., Ostermayer, F.W., Kohl, P.A., Ballman, A.A., and Logan, R.A., Holographic photoelectrochemical etching of diffraction gratings in *n*-InP and *n*-GaInAsP for distributed feedback lasers, *J. Appl. Phys.*, 1985, vol. 57, p. 39.
 157. Alferov, Zh.I., Goryachev, D.N., Gurevich, S.A., Mizerov, M.N., Portnoi, E.L., and Ryvkin, B.S., Diffraction lattices on the GaAs surface obtained by the method of interference photoetching, *J. Technical Physics*, 1976, vol. 46, p. 1505.
 158. Belyakov, L.V., Goryachev, D.N., Mizerov, M.N., and Portnoi, E.L., Some characteristics of diffraction lattices obtained by photoetching of semiconductor surface, *J. Technical Physics*, 1974, vol. 44, p. 1331.
 159. Kautek, W., Sorg, N., and Paatsch, W., Laser-induced electrodeposition of transition metals on silicon, *Electrochim. Acta*, 1991, vol. 36, p. 1803.
 160. Nánai, L., Hevesi, I., Bunkin, F.V., Luk'yanchuk, B.S., Brook, M.R., Shafeev, G.A., Jelski, D.A., Wu, Z.C., and George, T.F., Laser-induced metal deposition on semiconductors from liquid electrolytes, *Appl. Phys. Lett.*, 1989, vol. 54, p. 736.
 161. Sasano, J., Schmuki, P., Sakka, T., and Ogata, Y.H., Laser-assisted maskless Cu patterning on porous silicon, *Electrochem. Solid-State Lett.*, 2004, vol. 7, p. G98.
 162. Von Gutfeld, R.J., Acosta, R.E., and Romankiw, L.T., Laser-enhanced plating and etching: Mechanisms and applications., *IBM J. Res. Develop.*, 1982, vol. 26, p. 136.

163. Karlicek, R.F., Donnelly, V.M., and Collins, G.J., Laser-induced metal deposition on InP, *J. Appl. Phys.*, 1982, vol. 53, p. 1084.
164. Scheck, C., Liu, Y.-K., Evans, P., and Schad, R., Photoinduced electrochemical deposition of Cu on *p*-type Si substrates, *Phys. Rev.*, 2004, vol. B69, p. 035334(1–8).
165. Thietke, J. and Schultze, J.W., *Mikroelektrodenprozesse im fokussierten Laserstrahl. Elektrochemie und Elektronik. Dechema-Monographien*, B. 117. VCH Verlagsgesellschaft, 1989, p. 175.
166. Gelchinski, M.H., Romankiw, L.T., Vigliotti, D.R., and von Gutfeld, R.J., Electrochemical and metallurgical aspects of laser-enhanced jet plating of gold, *J. Electrochem. Soc.*, 1985, vol. 132, p. 2575.
167. Von Gutfeld, R.J., Gelchinski, M.H., Romankiw, L.T., and Vigliotti, D.R., Laser-enhanced jet plating: A method of high-speed maskless patterning, *Appl. Phys. Lett.*, 1983, vol. 43, p. 876.
168. Zouari, I., Pierre, C., Lapique, F., and Calvo, M., Maskless zinc electrodeposition assisted by pulsed laser beam, *J. Appl. Electrochem.*, 1993, vol. 23, p. 863.
169. Gusev, V.E., Kozlova, E.K., and Portnyagin, A.I., Role of thermal gradient effects in laser electrochemistry, *Soviet J. Quantum Electronics*, 1987, vol. 17, no. 2, p. 195.
170. Zouari, I., Lapique, F., Calvo, M., and Cabrera, M., Zinc electrodeposition assisted by pulsed YAG laser beam: Effect of hydrodynamic conditions, *J. Electrochem. Soc.*, 1992, vol. 139, p. 2163.
171. Datta, M., Romankiw, L.T., Vigliotti, D.R., and von Gutfeld, R.J., Laser etching of metals in neutral salt solutions, *Appl. Phys. Lett.*, 1987, vol. 51, p. 2040.
172. Hsiao, M.C. and Wan, C.C., The effect of pH on the localized etching process induced by laser irradiation, *J. Electrochem. Soc.*, 1994, vol. 141, p. 943.

Translated by T. Kabanova